NISTIR 89-4091

NEW NIST PUBLICATION

November 1989

BURNING, SMOKE PRODUCTION, AND SMOKE DISPERSION FROM OIL SPILL COMBUSTION

D. Evans
G. Mulholland
D. Gross
H. Baum
W. Walton

U.S. DEPARTMENT OF COMMERCE
National Institute of Standards and Technology
National Engineering Laboratory
Center for Fire Research
Gaithersburg, MD 20899

K. Saito

University of Kentucky
Lexington, KY 40506-0046

Sponsored by:
Minerals Management Service
U.S. Department of the Interior
Reston, VA 22091

U.S. DEPARTMENT OF COMMERCE
Robert A. Mosbacher, Secretary

NATIONAL INSTITUTE OF STANDARDS AND TECHNOLOGY
Raymond G. Kammer, Acting Director

LIST OF TABLES

		Page
Table 1.	Summary of Measured Burning Data in 1.2 m Diameter Pan	24
Table 2.	Properties of Test Liquids (Typical)	25
Table 3.	Energy Balance Estimates for the Steady Burning Period	26
Table 4.	Composition and Properties of Simulated Crude Oil	26
Table 5.	Comparison of Alberta Sweet Crude Oil Burning Data for 0.6 m and 1.2 m Diameter Pans	27
Table 6.	Effect of Layer Thickness on Smoke Emission from Alberta Sweet Crude Oil	28
Table 7.	Concentration of PAH in Alberta Sweet Crude Oil and its Burn Residue	29
Table 8.	Concentrations of Six PAHs Collected in the Vapor and Particulate Phases from the Combustion of Alberta Sweet Crude Oil	30
Table 9.	Concentration of PAH (Vapor and Particulate) Produced by the Combustion of Alberta Sweet Crude Oil	31
Table 10.	Comparison of PAH Content of Crude Oil, Oil Residue, and Smoke (Vapor and Particulate) per Gram of Fuel Consumed	32

LIST OF FIGURES

Page

Figure 1. Schematic diagram of the fuel level control device 33
Figure 2. Recorded Weight of Water Supplied to maintain oil level (Test A12) 34
Figure 3. Energy release rate per square meter for Alberta Sweet crude oil and pure hydrocarbons, tests A12, D01, T03 (10 mm layer thickness, fuel area 1.13 m^2) 35
Figure 4. Steady burning of toluene showing flame lifting 36
Figure 5. Radiant energy feedback to the fuel surface for Alberta Sweet crude oil and pure hydrocarbons, tests A12, D01, T03 (10 mm layer thickness, fuel area 1.13 m^2) 37
Figure 6. Smoke obscuration in stack for Alberta Sweet crude oil and pure hydrocarbons, tests A12, D01, T03 (10 mm layer thickness, fuel area 1.13 m^2) 38
Figure 7. Oil surface temperature at rim for Alberta Sweet crude oil and pure hydrocarbons, tests A12, D01, T03 (10 mm layer thickness, fuel area 1.13 m^2) 39
Figure 8. Temperature profile at center of pan (t=115 seconds), for Alberta Sweet crude oil and pure hydrocarbons tests A12, D01, T03 (10 mm layer thickness, fuel area 1.13 m^2) 40
Figure 9. Smoke/PAH sample collection system 41
Figure 10. Effect of oil layer thickness on energy release rate for crude oil fires 42
Figure 11. Effect of oil layer thickness on mass loss rate (fuel) for crude oil fires 43
Figure 12. Mass loss rate and extinction coefficients versus time for a crude oil fire 44
Figure 13. Comparison of gas chromatograph for Alberta Sweet crude oil and residue. Peaks: 1 Phenanthrene, 2-4 Methylphenanthrenes and 5-10 Dimethylphenanthrenes 45
Figure 14. Smoke aging and dilution chamber (CNC - Condensation Nuclei Counter) (TEOM - Tapered Element Oscillating Microbalance) 46
Figure 15. Effect of aging on mass distribution of crude oil smoke (log - probability plot) 47
Figure 16. Effect of aging on optical properties of crude oil smoke . . . 48
Figure 17. Schematic showing downwind evolution of smoke plume 49
Figure 18. Discretization of smoke into vorticity containing clumps. Horizontal density gradients induced vorticity . . . 50
Figure 19. Fluid motion induced by vortices is indicated by direction of arrows. Ground effect is represented by image vortices 51

Burning, Smoke Production, and Smoke Dispersion from Oil Spill Combustion

D. Evans, G. Mulholland, D. Gross, H. Baum and W. Walton
Center for Fire Research
U.S. National Institute of Standards and Technology
and
K. Saito
University of Kentucky

ABSTRACT

The combustion of crude oil layers floated on water were studied to assess the potential of using combustion to mitigate oil spills. Burning rates for n-decane, toluene and Alberta Sweet crude oil were measured in a 1.2 m diameter pool. These were used to estimate the energy transfer rate required to vaporize the fuel as part of an energy balance at the liquid surface. Smoke emission per unit of fuel consumed was dramatically reduced in the case of burning oil layers thin enough to cause boiling in the supporting water layer. A new aging/dilution facility is described that allows for measurement of optical properties and sedimentation velocities as the smoke ages. These characteristics are important in estimating smoke properties downwind of the oil spill fire. A formulation is presented that will provide for estimates of downwind particulate deposition of the fire smoke for a steadily burning oil spill.

Key words: crude oil; oilspills; polycyclic aromatic hydrocarbons; pool fires; smoke; fire plumes

1.0 BACKGROUND

In 1985, the Center for Fire Research (CFR) at the U.S. National Institute of Standards and Technology (NIST) began studies of oil spill combustion under support from the Minerals Management Service (MMS) of the U.S. Department of the Interior. This work seeks to quantify the processes involved in oil spill combustion on open waters and in water filled channels formed in broken ice including measurements of smoke production and prediction of smoke dispersal. Additional technical support from Environment Canada has allowed the study to be broadened to include in the scope chemical analysis of the oil, oil residue, and oil smoke.

The long range goal of the research program is to provide measurements and means to make quantitative predictions of (a) the fraction of oil in a spill that can be consumed by an in-situ combustion process, (b) the characteristics of the residual oil, and (c) the characteristics of the combustion products dispersed into the atmosphere. It is hoped that this information may be cast into a form that is usable by local officials and oil spill response professionals as part of the decision-making process in the event of an oil spill.

Last year's study was the first part of a two part study to quantify (a) the thermal properties and burning characteristics of the crude oil, (b) the physical and chemical properties of the smoke generated in the combustion process, and (c) the expected dispersal of the soot through the atmosphere and deposition down wind of the oil fires. These included results from experiments to quantify the burning of 0.60 m and 1.2 m diameter oil pool fires. Measurements of thermal radiation emission, smoke production and the polycyclic aromatic hydrocarbon (PAH) content of both the oil and the smoke were reported [1]. Initial calculations were presented to estimate the dispersal of smoke in the atmosphere characterized by a uniform wind velocity.

This year's effort emphasizes understanding of the crude oil vaporization process by burning both crude oil and selected pure hydrocarbons fuels in the 1.2 m diameter pool fire test facility. Soot production and chemistry during the rapid combustion period associated with boiling of the supporting water layer were measured to complement similar measurements collected prior to this boiling phase last year. Analysis of smoke dispersal in the atmosphere were continued by formulating a model for smoke particle settling time which is directly related to soot deposition on the ground remote from the combustion site.

2.0 BURNING CHARACTERISTICS

Previous experiments [1] were conducted to measure the burning characteristics of three types of crude oil floated on a water layer in a 1.2 m diameter pan. The earlier emphasis was placed on measuring the flame-plume temperature, energy release rate, and radiation feedback to the oil surface over a range of thickness of the oil layer. Also measured and reported were amount of oil residue remaining and the transient and steady-state burning patterns, including the nature of the vigorous burning phase involving boiling of the water sublayer. For Alberta Sweet, LaRosa, and Murban crude oils, it was

found that an initial oil layer thickness of 10 mm was sufficient to establish a period of quasi-steady state burning leading subsequently to a characteristic vigorous burning period just prior to flame extinction.

In this part of the study, the principal emphasis is on a better understanding of the heat balance at the burning oil surface in order to develop an appropriate model of the burning and extinction processes. The experimental arrangement and instrumentation were essentially identical to that previously described. Most measurements were made using a 10 mm thick layer of Alberta Sweet crude oil floated on water, with the major variables being the initial water temperature and the effect of wind. In addition, tests were conducted with 10 mm thick layers of the pure hydrocarbons n-decane and toluene, which were intended to represent the paraffinic and the aromatic components respectively in crude oil. More detailed measurements and analysis were made of the regression, i.e. burning, rate of the oil, the radiation feedback, and the extent of heat conduction into the oil and water layers during the burning periods. This analysis provides a background for predicting conditions under which a burning crude oil layer on water will self-extinguish prior to complete fuel consumption.

2.1 Burning Experiments

A summary of the principal data recorded in this test series is given in Table 1. Certain features of the test setup and results are of particular interest:

The regression rate of the burning oil was determined by measuring the rate at which water was supplied to the 1.2 m diameter test pan in order to maintain the oil surface exactly 12 mm below the top of the pan rim. The level control device is shown schematically in Figure 1. A sensitive diaphragm-type pressure transducer (No.1) is connected to a pressure tap near the bottom of the test pan. When a slight decrease in pressure corresponding to the burning of oil is noted, the operator manually adjusts valve No.2 to permit water to flow from the sump pump in the auxiliary reservoir to restore the initial test pan pressure. The decrease in the weight of water which is recorded as the output of pressure transducer No.2, corresponds to the fluid volume required to maintain the prescribed depth in the test pan. Since the oil in the pan is less dense than water, a slight error (averaging about 8% of the oil depth) will be introduced unless compensated by a predetermined amount based on the oil thickness and the difference in specific gravities of oil and water. Although not compensated for during the test, the effects of density difference were included in the calculation of burning rate.

Figure 2 is an example of the recorded weight of water supplied in Test A12 (from output of pressure transducer No.2) and illustrates the increased burning rate during the vigorous burning period near the end of the test.

The recorded energy release rate for the Alberta Sweet crude followed the same pattern as in earlier tests, i.e., a rapid rise to approximately 1.4 MW followed by a slight decrease over a 1.5 min period to about 1.1 MW and then rising to a peak value of about 2.8 MW during the vigorous burning period (see Figure 3). The pure compounds toluene and n-decane did not display the same

changeover to intense burning and corresponding water-boiling phenomenon as the Alberta Sweet crude although there was noticeable boiling for an extended period over the surface of the decane. This is ascribed to the much higher oil surface temperature (corresponding to the higher boiling point) for the crude oil at this stage of burning. The decane energy release rate increased fairly steadily to a peak of 2.6 MW followed by a steady decline whereas the toluene approached and maintained a steady-state energy release rate of only 1.8 MW. Both the toluene and the decane were observed to burn as flame sheets around the perimeter of the test pan with very little or no flaming at the central core. This is ascribed to the greater vapor production ratio for the pure hydrocarbons. In the case of toluene, flame lifting at the rim was quite pronounced; this may be seen in the close-up photograph of the liquid surface in Figure 4.

As shown in Figure 5, the recorded peak level of radiant energy feedback to the center of the liquid surface was lowest for toluene (23 kW/m^2) and highest for the Alberta Sweet crude (65 kW/m^2). As noted in the previous report [1], the feedback radiation did not follow the same temporal pattern as the energy release rate, and this is in part a consequence of the different quantities of generated smoke, which affects both the absorption of radiation by and the emission of radiation from the flames. Also shown in Figure 5, for direct comparison with the feedback at the center for Alberta Sweet crude, is the recorded level of radiation energy feedback near the rim of the pan. At levels of radiant energy feedback below approximately 10 kW/m^2, flaming could not generally be sustained.

The recorded smoke obscuration in the stack (see Figure 6) confirms graphically the visual test observations in which very little smoke was noted throughout the test for the decane and very heavy smoke for the toluene. The progressive increase in smoke generation for the Alberta Sweet crude can be attributed to the changing composition of the crude oil toward the heavier fractions with decreased combustion efficiency.

The measured oil surface temperature provides a good indication of the pattern of burning. In Figure 7 are plotted the temperatures at the oil surface near the rim where the fuel vapor from the burning liquid and air are able to mix to produce the basic flame structure. The constant temperature portions correspond to the boiling points of 111 °C for toluene and 174 °C for decane are clearly observed. The steadily increasing oil surface temperature for the Alberta Sweet crude demonstrates the progressive boiling off of the lighter fractions which have lower boiling points. This is a reasonable and expected behavior, in contrast to a constant temperature phenomenon [2].

Using the previously described thermocouple rakes [1], temperature measurements were recorded within the oil layer, in the fuel-rich vapor above the oil, and in the water sublayer. This provided temperature profile data at selected times such as that shown in Figure 8 for three liquids at 115 sec, where the measured data points were connected by straight line segments. However, due to the uncertainty in establishing the free surface of the liquid closer than ±1.6 mm, the temperature profiles may appear slightly displaced relative to the original oil surface. These data illustrate that at the center of the pan, the temperature immediately at and above the surface of the toluene is 111 °C

corresponding to toluene at its boiling point. Likewise, the space directly above the boiling decane liquid consists of decane vapor at 174 °C. At 115 seconds, these pure compounds are in the middle of the characteristic steady burning phase and the flames are mainly confined to an envelope close to the rim where air is available for burning. At the same time in the burning period of the Alberta Sweet crude (115 sec), the oil surface has reached a temperature of approximately 250 °C to 300 °C and is continuing to increase steadily as the lower boiling point fractions disappear.

The main effects of a 1 m/s or 2.5 m/s wind blowing across a burning pool of Alberta Sweet crude was (a) to deflect the flames as much as 45° from the vertical and (b) to increase the burning rate and reduce the burning time noticeably (see table 1).

Over the initial water temperature range explored (5 °C to 28 °C), there was no pronounced, systematic effect on measured temperature in the flame, thermal radiation, burn time or residue remaining. This is not surprising since the heat loss by conduction is relatively small and occurs in a thin surface layer, so that the cooler substrate has negligible effect until burning is nearly complete.

2.2 Energy Balance

For estimating the energy balance, discussion will be limited to the quasi-steady burning period prior to the violent burning phase involving the boiling of the water sublayer. Even so, conditions at the burning oil surface, plus the attendant uncertainties in experimental measurement of irradiance, and of temperature and level control within a few millimeters, provide a severe measurement and analytical challenge. In the violent burning stage, this is further complicated by the motions of boiling water and splattering oil droplets, possibly resulting in water-oil emulsions.

In simple qualitative terms, the net rate of energy received at the oil surface may be equated to a series of energy rate terms:

$$Q_i - Q_{rr} = Q_v + Q_c$$

where Q_i is the rate of radiant energy incident on the oil surface, Q_{rr} is the rate at which energy is reflected or re-radiated, Q_v is the energy flux required to vaporize the oil, and Q_c is the net energy flux conducted or convected away from the oil surface. Not included here are any energy gains or losses associated with the vessel walls and chemical changes within the oil.

In order to make energy balance estimates, thermal properties of the test liquids are required. Values were either obtained or derived from available reference sources and are listed in Table 2.

During the quasi-steady burning period, the radiant energy flux incident on the surface of the Alberta Sweet crude oil at the center was found to rise from 40 to 65 kW/m^2 whereas the radiant flux energy at the rim remained fairly constant at 18 kW/m^2. It is not clear if the mean levels of radiant energy flux within

a much larger pool would be closer to the values at the center or at the rim. Although the rate of energy reflected and re-radiated is important, this could not be estimated due to lack of data on spectral and total absorptivity.

From the recorded temperature profiles, temperature gradients at the oil surface were determined and estimates made of the extent of heat conduction to the interior of the oil. As shown in Table 3, the maximum temperature gradient in the oil was 29 degrees C/mm corresponding to a heat loss by conduction of 2.5 kW/m^2. The accuracy of this measurement is estimated to be ±20 percent. For estimating the thermal conductivity of the Alberta Sweet crude, an average boiling point of 250°C was selected for the steady-state burning period. Also listed in Table 3 is the energy rate required to vaporize the oil as computed from the measured liquid regression rate and the heat of vaporization at the boiling point. For the Alberta Sweet crude, the heat of vaporization is a changing function since there is a progressive shift from the lowest to the highest boiling point fractions during the burning process. An effective composite heat of vaporization may be estimated based on mass fraction if the crude oil is assumed to consist of paraffinic and aromatic components as illustrated in Table 4. In this case the rate of energy required for vaporization during the quasi-steady state burning period is approximately 6.7 kW/m^2, (calculated from the product of measured surface regression rate, fuel density and heat of vaporization).

If the rate of energy loss is in the form of convection, it may be appreciable. For example, a 3 mm thick layer of crude oil exposed to a temperature difference of 150 °C could transfer approximately 10 kW/m^2, (based on a heat transfer coefficient of 0.075 kW/m^2K).

In the case of the pure liquid hydrocarbons n-decane and toluene, a region of constant temperature approximately 3 to 5 mm thick exists in the vapor zone directly above the liquid surface. However, a constant temperature ("homothermal") liquid layer such as noted by Burgoyne and Katan [3] and by Blinov and Khudyakov [4] was not observed. In their 1947 paper, Burgoyne and Katan suggested that distillation may occur at the bottom of such a liquid layer and that the vapor bubbling up could provide a stirring action (with the required nuclei provided along the vessel walls). For the Alberta Sweet crude oil, no distinct constant temperature liquid layer was discernible. The computed rates of energy conducted into the pure hydrocarbons ranged from 2.3 to 3.3 kW/m^2, whereas the energy rate required for vaporization varied from 15.1 to 19.1 kW/m^2. In these cases, it is also not possible to provide a complete and consistent heat balance in the absence of more confirmation on the magnitudes of the energy rate terms associated with convection and with reflection and re-radiation.

2.3 Burning of Thin Oil Layers

Oil spill combustion in which the oil layer is being churned by the boiling of a supporting water layer may be the most prevalent conditions for thin oil slicks and the most beneficial because of relatively lower smoke yields when combustion can be maintained. This type of combustion condition was observed during the latter part of each crude oil burn in this study. Churning of the water and oil interface and possible emulsification eventually leads to flame

extinction as the oil is cooled by the mixing process sufficiently to prevent the flame sustaining fuel vaporization. Thus heat transfer processes in this complicated burning situation determine both the amount of water mixed with the oil vapors during the combustion and the amount of oil left on the water surface after flame extinction.

To understand the combustion process better a simple transient conduction model with a specified burning surface temperature was formulated as an attempt to predict the onset of boiling in the water supporting layer beneath the burning oil layer. Experimentation was performed with pure hydrocarbon fuels and three types of crude oil. It was found that there was no reasonable choice of physical properties for this simple combustion model that would consistently predict the onset of water boiling for either a bench scale or large scale pool fire situation. In all cases the calculated time to boiling was much greater than that observed in experiments. A more complete model that includes in-depth radiation adsorption as well as conduction into the liquid is being formulated.

3.0 SMOKE CHARACTERISTICS

In the previous study [1], the total smoke particulate and its chemical content were measured for smoke emitted during the steady burning phase for a 30 mm thick layer of Alberta Sweet crude oil on water. While collecting smoke during the steady burning phase simplified the measurements and allowed good repeatability, it ignored the effects of oil layer thickness and boilover on smoke emission. To complete the laboratory scale study of smoke, the effects of oil layer thickness on the total smoke emitted and its chemical content were studied. The procedure for collecting a representative fraction of smoke throughout the entire burning period is described below. In the previous study, we did not include a chemical analysis of the PAH (polycyclic aromatic hydrocarbon) content of the crude oil and in the residue. Such measurements are included in this study to provide the necessary data for assessing the environmental impact of burning crude oil.

As smoke rises in a plume from the burning oil, the individual agglomerate particles will collide and stick together forming larger agglomerates. This process will continue to take place as the smoke plume moves downwind. There is very little information regarding the effect of the agglomeration process on the properties of the smoke. Properties of keen interest in regard to environmental effects are changes in the optical properties of the smoke and the change in the aerodynamic size of the smoke particles. The optical properties are of concern in regard to visibility reduction caused by the smoke and the absorption of solar radiation in the atmosphere. The aerodynamic properties of the smoke are of interest in regard to the deposition of the smoke. As will be discussed in the Particulate Settling Analysis section of this paper, the smoke deposition is affected by the high mass loading of the smoke inducing a cloud settling effect as well as by the settling velocity of the individual agglomerates near the ground. The design of a Smoke Aging/Dilution facility is described and preliminary results on the effects of agglomeration on the optical properties and the aerodynamic properties of smoke are given.

3.1 Smoke Emission Measurements

Smoke samples were collected and diluted using a gas sampling system shown in Figure 9. The smoke was drawn through an isokinetic sampling probe into a dilution section where it was diluted two to one on a mass basis with approximately 0 °C clean air. Diaphragm pumps pulled the diluted smoke through two filter sets arranged in parallel. Each filter set consisted of a teflon[1] filter, 37 mm diameter, followed by a polyurethane foam vapor trap contained in a glass tube 30 mm diameter and 150 mm long. All teflon filters, polyurethane foams and glass tubes were prewashed to remove organic contaminants. The parallel filter sets allowed simultaneous collection of soot and PAH on the two teflon-polyurethane filter sets. Smoke sampling flow rates averaged approximately 10 liters per minute. In contrast to crude oil burns conducted previously [1], when samples were collected for short periods during the steady state burning phase, smoke was sampled continuously from ignition until burning was completed. In order to collect sufficient mass for analysis, multiple burns were necessary for the 2 mm, 3 mm, and 5 mm oil layer thicknesses. Upon completion of a burn or series of burns, the teflon filters were weighed and sealed in petri dishes, while the polyurethane foam-glass tube combinations were stored in aluminum foil. Both teflon filters and polyurethane foam were then stored under dry ice until ready for analysis. Soot samples for thermal-optical analysis of elemental versus organic carbon content were collected on quartz fiber filters which had been prefired at 700°C for 4 hours. The same collection and dilution system was used for the quartz filters except that polyurethane filters were not included downstream of the quartz filters. Because the thermal-optical technique requires much less soot per filter, smoke sampling flow rates averaged about 2 liters per minute.

In addition to the teflon, polyurethane and quartz filters, samples of the crude oil before the burn and the residue after the burn were also collected for chemical analysis. An oleophilic polypropylene batting was used to soak up the burn residue for weighing. The percent of oil burned was calculated based both on the mass loss during the burn and on the mass of the burn residue. Both methods agreed within a few percent except for the 2 mm layer, for which the first method gave 63% and the second method gave 54%. The results of the second method are given in Table 5.

The effect of oil layer thickness on the heat release rate and on the burning in the 0.6 m diameter pan rate are illustrated in Figures 10 and 11. The 5 and 10 mm thick pool burns have a relatively steady burning phase with a 0.2 MW heat release rate followed by rapid burning with a 0.6 to 0.75 MW heat release rate as the water under the oil begins boiling. Apparently the boiling of the water causes small droplets of crude oil to be emitted from the surface. The rapid boiling phase lasts up to about one minute. For the 2 and 3 mm thick layers, there is no steady burning phase. The time to boilover increases with

---

[1] Certain commercial equipment, instruments, and materials are identified in order to adequately specify the experimental procedure. Such identification does not imply recommendation or endorsement by the National Institute of Standards and Technology, nor does it imply that the materials or equipment identified are necessarily the best for the purpose.

oil layer thickness from about 35 seconds for the 2 mm layer to about 270 seconds for the 10 mm thick layer (Table 5). The smaller the layer thickness, the larger the fraction of the mass loss occurring during the boilover phase. While the heat release rate varies with layer thickness and time, the effective heat of combustion is relatively constant throughout each test and over the ranges studied with a value of 35 to 40 MJ/kg. This represents 80% to 92% of the estimated net heat of combustion, 43 MJ/kg.

A comparison between these results for a 10 mm thick layer in an 0.6 m pan and the results for a 1.2 m diameter pan [1] are contained in Table 5. The steady state heat release rate for the 1.2 m diameter pool, 1.00 MW/m^2, is about 50% greater than for the 0.6 m diameter, 0.67 MW/m^2. The mass burning rate shows a similar trend increasing from 15 g/m^2s to 22 g/m^2s with increasing pool size. This result is expected in view of the relationship between burning rate and pool diameter established by Blinov and Khudyakov [4] and analyzed by Hottel [5]. Other noteworthy effects of pool size include a smaller residue percentage at the larger pool size and a significantly shorter time to boilover, 130 seconds for 1.2 m diameter pool, compared to 271 seconds for the 0.6 m diameter pool with 10 mm layer depth. About 60% of the mass loss occurred during boilover for the 1.2 m pool compared to only about 33% for the 0.6 m diameter pool.

The transmittance, I/I_0, of a He-Ne laser, $\lambda = 633$ nm, through the smoke in the stack was monitored with a photometer. The laser beam is located about 1 m above the sampling probe. The light extinction coefficient, k, is derived from the light transmittance via Bouguer's law, $I/I_0 = e^{-kL}$, where L is the pathlength through the stack. The time dependence of k is illustrated in Figure 12 for a 10 mm oil burn. In the region where the mass loss rate of the fuel is a maximum, the smoke extinction coefficient k is actually decreasing. It appears that the smoke emission is greatly reduced during this rapid burning phase. The quantity σ_f, the extinction cross section per unit fuel mass loss, is a convenient relative measure of the smoke emission.

$$\sigma_f = k/(\dot{m}_f/\dot{V}),$$

where $\dot{m}_f$ is the fuel mass loss rate and $\dot{V}$ is the volumetric flow rate through the duct. The quantity σ_f is proportional to the smoke yield ϵ, defined as the mass of smoke aerosol produced per gram of fuel consumed. The plot in Figure 12 clearly shows a dramatic decrease in σ_f by about a factor of five during the rapid fuel burning. This effect of decreasing σ_f at the time of the maximum burning is observed for all layer thicknesses.

The smoke yield results are summarized in Table 6. It is seen that the smoke yield ϵ increases by more than a factor of two from 0.035 to 0.080 as the fuel layer thickness is increased from 2 mm to 10 mm. The value of σ_f also increases by almost a factor of two from 0.33 m^2/g to 0.65 m^2/g as the thickness is increased from 2 mm to 10 mm. The quantity σ_s, which is the specific extinction cross section per unit mass concentration of smoke, is in the range 7 to 9 with no definite dependence on oil layer thickness. The experimental variability is larger in these experiments compared to the steady state experiments performed last year because of the large change in burning

rate and smoke emission during the burn. Also, there is evidence of large oily droplets on the sampling probe and just downstream of the bend in the sampling probe. These droplets may flow through the laser beam, but possibly only a small fraction are making it to the filter.

3.2 Chemical Analysis

Smoke samples were collected on quartz filters as described in the preceding section and sent to a contract laboratory for the thermal-optical analysis for organic/elemental carbon [6]. The organic fraction of the sample is determined by heating the sample in pure helium in four temperature steps up to 770 °C. The remaining carbon, the so called elemental carbon, is then oxidized by introducing 2% O_2 into the gas stream. The elemental carbon fraction of the smoke was in the range 79% to 86% without any significant trend with oil layer thickness. The heavier deposits were observed to be very uneven across the filter surface. These results are to be compared with values over 90% obtained for the collection of smoke last year from the steady burning phase. This year the samples were collected over the entire burn. The lower values observed in this years study may be a result of fuel droplets being emitted from the surface and collected during the rapid boiling phase.

The PAH analyses of 11 filter and corresponding polyurethane foam samples were performed by the Center for Analytical Chemistry at NIST and by Environment Canada at Ottawa. In addition, PAH analyses were performed on 5 crude oil samples and on 7 burn residue samples. The goal of this portion of the research was to assess the effect of oil layer thickness on the PAH emission and on the PAH content of the residue. The sample procedure was essentially the same as previously reported [1]. The teflon filters and polyurethane foam samples at NIST were spiked with appropriate amounts of an internal standard solution containing phenanthrene-d_{10} and 1-n-butylpyrene. Agreement within about 10% was obtained between the concentrations calculated using the two standards suggests that there were no significant losses of the more volatile species relative to the less volatile standard, 1-n-butylpyrene.

The analysis at NIST involved gas chromatography with flame-ionization detection (GC/FID). Extensive pre-separation using liquid chromatography was necessary to isolate the PAH-rich fraction when using this method [7]. At Environment Canada, mass detection is used for quantifying the individual PAH species, which has the advantage of requiring a minimum amount of pre-separation. A total of five internal standards are used for accounting for the variability in the recovery factor with the size and structure of the PAH. One advantage of the GC/FID system for the nominally 10 mg smoke samples is its factor of 10 higher sensitivity than the mass detection method.

Essentially the same preparation method was used for the crude oil and oil residue samples except that the silica cartridges were not used in the pre-separation procedure. The results for the crude oil and residues are summarized in Table 7. Generally, the PAH content in the crude and the residue were similar, which is more apparent when comparing the chromatograms for the oil and residue (see figure 13). Over 90% of the PAH content are three membered rings with high concentrations of phenanthrene, methylphenanthrene, and dimethylphenanthrene. Environment Canada found that the concentrations of

four and five membered rings were less than the three membered ring by a factor of 10 or more. The recovery percentages for the spiked components were uncertain because of interferences. The GC/FID method used at NIST was unable to quantify PAHs with more than 3 rings due to the complicated structure in the chromatogram in this region. Both laboratories agreed to within 10 - 20% for the concentration of phenanthrene, which was the only PAH in the oil samples measured by both laboratories.

Table 8 includes the masses of six PAHs measured in the extracts of five polyurethane foam plugs positioned downstream of the teflon filter. These results would include both PAH inherently in the vapor phase, as well as those species that were desorbed from the particles on the filter and subsequently collected on the foam. The top and bottom sections of PU-12 were processed separately to determine whether any breakthrough of PAH had occurred. No significant concentration of any PAH was observed in the bottom section, suggesting that PAH breakthrough was not a problem in this study. Comparison of the masses of PAH in the foam and filter extracts shown in Table 8 indicate that a major fraction of three of the PAHs, all three ring compounds, were collected in the vapor phase. The agreement between the two laboratories was within the 10 - 20% measurement uncertainty as indicated by the good agreement between the results by NIST on sample 5 and the results by Environment Canada on sample 6, which was collected simultaneously with 5 and had almost the same filter mass. The distributions between particle and vapor phase were sample dependent with the smaller layer burns having a larger vapor component. The cause of this sample dependence is probably desorption of the PAH, since the total collection times were three to five times longer for the 2 mm and 3 mm burns compared to the 5 mm and 10 mm burns. An individual burn was shorter for the 2 and 3 mm burns but many burns (12 mm for the 2 mm layer and 7 mm for the 3 mm layer) were required to obtain enough smoke sample for analysis. If one combines the results for the vapor and the particulate phases, there is no systematic effect of layer thickness on the 3 ring PAH content.

The results on the total PAH, both in the particulate and vapor form, per unit smoke mass are contained in Table 9. There is some variability from sample to sample but no obvious dependence on the layer thickness. That is, both the total amount of the PAH and the type of PAH appears to be independent of the thickness of the layer being burned. The results are also similar to the results for the collection of the smoke during the steady burning of a 30 mm pool carried out last year. The concentration of phenanthrene and anthracene are low for the 30 mm burn, but this is to be expected, since only the particulate was collected in this sample. The low concentration of methylphenanthrene relative to phenanthrene indicates that 10% or less of the smoke is unburned crude oil. This result is consistent with the high elemental carbon fraction of the smoke discussed above.

In Table 10, all the results are summarized on a per gram of crude oil consumed basis for ease in estimating the environmental impact. It is noteworthy that the burning of one gram of crude oil produces less total PAH (the sum of the residue plus smoke/vapor) than is in the original crude oil. However, the concentration of PAHs with 5 or more rings, which includes benzo[a]pyrene, is 10 to 20 times greater in the smoke compared to the fuel. The crude oil and the residue have the same relative concentration of the various classes of

PAHs, and the reduction in the overall amount arises from the fraction of the oil burned. While about 90% of the PAHs for the oil and residue have three rings, the PAH content of the smoke/vapor is equally divided among three rings, four rings, and 5 or more rings. The low total concentration of PAH at small layer thickness is primarily the result of the relatively low smoke yield under these conditions. While the smoke/vapor emission is a minimum for the smallest thickness, the residue is a maximum.

The measured total PAH content in the smoke from crude oil fires ranging from 330 to 770 μg PAH/g crude oil (see Table 10) can be put in perspective with comparisons of emissions from wood fueled residential heating equipment. The literature contains some information about PAH content of smoke from wood combustion in heating equipment. Measured PAH emission from wood stoves range from 1 to 370 μg PAH/g dry wood with a typical value of 40 μg PAH/g dry wood [8]. Typical yields of PAH compounds from fireplaces are 29 μg PAH/g dry wood [8].

The above information suggests that the PAH emission from burning of crude oil spills is order 10 times that produced during the controlled burning of a equal weight of wood in heating equipment and fireplaces. Using a factor of 10 for the relative PAH production, the burning of one gallon (3.8 liters) of crude oil would produce the same total PAH emission as the burning of three fireplace size logs (0.2 m diameter by 0.5 m long).

3.3 Aging and Dilution Chamber

In a smoke plume, the optical and physical properties of smoke change as the smoke ages. Close to the fire source, these changes occur in hot, fresh smoke, but downstream in the plume, changes also occur in the cooler smoke which may or may not be diluted. In order to study how these changes affect properties, such as the light extinction and size distribution of the smoke particles, an Aging and Dilution chamber has been designed. For the hot, fresh smoke, the smoke box must rapidly capture a sample and age it at the collection temperature and pressure for several hours while measurements are collected. For cooler, more diluted smoke, the chamber must dilute a warmer smoke sample and age it at steady conditions until measurements are taken. While the fresh samples require a heated box, the cooler samples need an efficient dilution system. Both samples require a chamber that can be tightly sealed after a sample has been rapidly pulled into the box. The design must include windows for light transmission measurements and sampling ports for mass and number concentration and size distribution determinations. Instead of adding makeup air as the samples are withdrawn and diluting the smoke sample, the chamber includes a large volume piston which moves down to compensate for the sample volume extracted. All these requirements for aging fresh, hot smoke and cooler, dilute smoke are incorporated in the design of the Aging and Dilution Chamber (see Figure 14).

The chamber is a 1 m^3 aluminum box which has been lined with stainless steel to reduce corrosion from the hot combustion gases. Forty eight mica resistance strip heaters are attached to the aluminum walls which evenly distribute the heat for wall temperatures up to 150 °C. The intake duct work and valve can also be electrically heated. For experiments which require cooler or more

dilute smoke, dilution air can be added via a port in the intake line. The port is designed to allow adequate mixing of the dilution air and smoke before entering the chamber. Orifice flowmeters permit measurement of the inlet, exhaust and dilution air flow rates. To allow for rapid filling of the chamber, a variable speed exhaust fan pulls smoke through the chamber at flow rates up to 8 m^3 per minute. Using the variable speed fan and inlet tips of diameters ranging from 1.5 to 10 cm, the inlet velocity can be matched with the stack velocity for isokinetic sampling. The smoke enters and exits the chamber through 10 cm diameter stainless steel duct work. After the chamber is filled and well mixed, two stainless steel butterfly valves, one on the inlet and one on the outlet, are simultaneously closed to capture a 1 m^3 sample. A 100 liter piston which is located on top of the chamber allows the volume of the chamber to be reduced as samples of smoke are withdrawn from any of the 20 sampling ports. A pair of the sampling ports have been adapted for a three wavelength photometer for extinction measurements. Some of the other instruments which will be used with the chamber include the tapered element oscillating microbalance, a seven stage cascade impactor, a condensation nuclei counter and the transmission cell-reciprocal nephelometer.

For the preliminary work with crude oil fires, light extinction, mass concentration and size distribution data were collected with the photometer, microbalance and impactor. The photometer, which is similar to Cashdollar's [10] design, consists of a white light source, two beam splitters, three interference filters and three photodiodes. Mounted on opposite walls of the chamber, the light source and the receiving optics are separated by pathlength of 1.1 meters. Measuring the amount of light extinction at 450, 630 and 1000 nm, the photometer allows calculation of the extinction coefficient at each wavelength. In order to calculate the amount of extinction per unit mass concentration of smoke, the mass concentration of the smoke in the chamber is determined with the Tapered Element Oscillating Microbalance (TEOM). Approximately two liters of smoke are necessary to make a mass concentration measurement.

While the photometer measures light extinction and the TEOM determines mass concentrations, a seven stage cascade impactor provides size distributions of the fresh smoke, as well as the aged smoke. The cascade impactor aerodynamically classifies the smoke aerosol by allowing the smoke to cascade through succeeding orifice stages with successively higher orifice velocities. The larger particles are inertially impacted on the early collection stages and successively smaller particles are inertially impacted on following stages. Particles smaller than 0.4 μm are collected on a backup filter. The particles are classified into seven bins ranging from 0.4 μm to 10 μm.

A preliminary series of experiments were performed to look at the effect of aging on smoke properties. Samples of crude oil smoke were collected and aged for up to 150 minutes, during which time mass concentration, size distribution and light extinction measurements were obtained. The mass concentration peaked at about 200 mg/m^3 just after the chamber was filled with smoke. Generally, the mass concentration decreased by a factor of about 2 over the 150 minute aging period due to settling given the inferred velocities. The TEOM measured the mass concentrations every 10 minutes throughout the aging experiment. As the crude oil smoke was aged for 90 minutes, the median aerodynamic diameter

based on a mass weighting increased from about 0.8 μm to about 1.1 μm (Figure 15). The term aerodynamic diameter means that the particle settles with the same velocity as a unit sphere with this diameter. The 0.8 μm and 1.1 μm aerodynamic diameters correspond to settling velocities of 0.03 mm/s and 0.06 mm/s, respectively. Aging the smoke for 150 minutes resulted in a mass median diameter of about 2.5 μm.

The specific extinction area, σ_s, at 450, 630 and 1000 nm did not change significantly over a 90 minute aging experiment (Figure 16). Three wavelength extinction data were collected every 10 minutes throughout the aging period. The mean value for σ_s were 5.1 (1000 nm), 8.0 (630 nm), and 9.7 (450 nm). In last year's study, we found σ_s equal about 10 based on laser transmittance (λ=633 nm) through the stack for the steady burning phase. We obtained a value of about 8 based on data collected over the entire burn.

We are planning more studies utilizing the aging facility to include the determination of the agglomeration coefficient using the condensation nucleus counter, the settling velocity of the smoke, as well as the effect of aging on the size distribution and optical properties.

3.4 Discussion

The major focus of this part of the study is the effect of oil layer thickness on the smoke emission and its chemical properties. We find that the smoke yield, ϵ, increases from 0.035 g smoke/g fuel to about 0.080 g smoke/g fuel as the layer thickness is increased from 2 mm to 10 mm. We also observe that for the 2 mm and 3 mm layer thicknesses about 65% of the mass loss takes place in the boilover mode, while for the 10 mm thickness only about 33% of the mass loss occurred during the boilover. We suspect that the high water vapor emission during the boilover phase is responsible for the decreased smoke emission. For a 10 mm burn, we observe a reduction in σ_f, which is proportional to ϵ, from a peak value of about 1.2 during the steady burning phase to a value of 0.2 -0.4 during the boilover phase. This is another indication that the boilover is affecting the smoke production. In a follow on study, we plan to sample only the smoke produced during the boilover phase to better characterize the amount emitted and its properties.

In a review of the effect of water on combustion [11], Dryer indicates that the presence of water in residual water/oil emulsion can lower the particulate emission. The reduced flame temperature resulting from the higher heat capacity of water vapor compared to nitrogen is thought to be an important factor regarding soot emission. Schug et al. [12] have demonstrated that the reduction in the sooting tendency of an ethene laminar diffusion flame with added water vapor is primarily a thermal effect. Rao and Barden [13] report that the amount of soot leaving the flame decreases and that the peak flame temperature decreases with increasing water vapor concentration for laminar burning of diesel emulsion. In contrast, the peak flame temperature measured with a thermocouple for the 1.2 m diameter pool of Alberta Sweet crude oil increased by about 100 $^{\circ}$C at boilover rather than decreasing as in the laminar flame studies [12,13]. However this boilover effect is not simply water vapor addition with everything else held fixed. The boilover phenomenon increases the fuel generation rate several fold and also appears to enhance the mixing of

air and fuel droplets near the fuel surface. While we expect boilover to be important in reducing soot emission at realistic scale fires, field scale, and additional laboratory scale turbulent burning studies will be essential in understanding the scaling effects because of the complex coupling between boilover, fuel generation rate, mixing, and radiation feedback to the surface.

While the total smoke emission is significantly affected by the layer thickness, it appears from measurements made both at NIST and Environment Canada that both the total amount and the distribution of PAHs per gram of smoke is not greatly affected by the layer thickness. Of course, since less smoke is emitted per gram of fuel consumed, the yield of PAHs is lower for the smaller layer thicknesses. The total PAH emitted per gram of fuel consumed is on the order of a factor of two-three times less for the 2 mm layer compared to the 10 mm layer.

In this study we have collected both the vapor and particulate phase PAHs and find that a majority of the three ring PAH may be in the vapor phase. For a collection temperature of about 35° C, we find that 20 to 60% of anthracene is collected on the filter and 60 to 100% of fluoranthene is collected on the filter. These values are to be compared with 90% retention for anthracene and a 100% for fluoranthene reported by Longwell [14] for 40° C collection temperature. Clearly, there are effects other than the collection temperature controlling the fraction of PAH on the filter. We find that desorption can be significant and one also expects the mass concentration of the smoke to play an important role.

The PAH concentrations for the Alberta Sweet crude oil and the burn residue are very similar; in fact, it might be possible to use the PAH distribution in the burn residue to identify the crude oil that was burned. In the higher vapor pressure C_1 to C_4 alkanes and the mono-ring aromatics including benzene, toluene and xylenes, it has been reported by Evans et al. [15] that the residue is depleted relative to the crude oil. The PAH analysis at NIST indicated a high concentration of alkylphenanthrenes in the oil and residue but a very small concentration in the smoke. This indicates that very little unburned oil becomes deposited on the smoke. The Environment Canada data indicate a very low concentration of 4 and 5 ring PAHs. The analysis of PAH in the oils and residues was much more difficult than the smoke because of components in the oil interfering with the chromatographic separation of the PAH.

This may be the most complete and careful study regarding PAH emission from a fuel. This data should be useful as a first step in assessing the environmental impact of burning crude oil at sea. There is now a critical need for smoke data at the field scale for realistic oil layer thicknesses. The data at 0.6 and 1.2 m scale indicates a decrease in unburned oil residue and a decrease in smoke yield as the pool diameter increases. These trends may continue to field scale, but other combustion effects involving radiation that are significant only at field scale require testing to be performed at that scale.

Preliminary data obtained with the Aging/Dilution facility suggests that particle agglomeration leads to about a 30% increase in aerodynamic particle size over a 90 minute aging period. The actual smoke from a large fire would

entrain air and be diluted so that 90 minutes of aging in the chamber could correspond to a day of aging in a smoke plume. This observed increase in particle size with aging does not seem to affect the specific extinction areas measured at 450, 630, and 1000 nm. This result is consistent with the idea proposed by Mulholland et al. [16] that for low density agglomerates made up of spheres much smaller than the wavelength of light the optical absorption per unit mass would be independent of agglomerate size. The aging/dilution facility will be used to measure the settling velocity of the agglomerates and the settling rate of a cloud of particles. We expect that cloud settling to be the controlling mechanism for particle deposition as discussed in the next section.

4.0 PARTICULATE SETTLING ANALYSIS

The purpose of this section is to develop a method for solving the equations which govern the evolution of a smoke particle plume from the point at which it is injected into the atmosphere until it is finally deposited on the ground. The mathematical model on which the analysis is based is a special case of that developed by the authors in the previous portion [1] of this ongoing research, and will not be re-derived here. The principal assumptions underlying the model are:

1) The fire generating the smoke and hot gases is burning steadily.

2) The injection altitude and particle mass flux associated with the fire are known.

3) The gas temperature in the buoyant plume equilibrates with the atmosphere before any significant particle settling begins.

4) The ambient wind speed is much larger than the velocities induced by the negatively buoyant smoke particle plume.

5) Individual particle settling velocities are much smaller than the collective effects represented by the smoke particle plume.

6) The stratification of the atmosphere plays no role in the settling process.

The last assumption limits the injection altitude for which the analysis is valid to at most one kilometer. The determination of the injection altitude itself is not part of this analysis, although it does fit within the framework of the mathematical model developed earlier. The goal of the present study is the ability to predict the downwind deposition pattern of the smoke particulate on the ground. The controlling parameters are the injection altitude and initial cross-section area of the plume, the particulate mass flux, and the ambient wind velocity.

To proceed, we introduce a cartesian coordinate system X,Y,Z as shown in figure 17. The variable X increases in the direction of the ambient wind, Z is directed vertically upward, and Y is horizontal coordinate perpendicular to the other two. Let U,V and W be the air velocity components in the X,Y and Z

directions respectively. In this model U is the ambient wind speed and is presumed known. The smoke particulate is described in terms of a mass density ρ_p, mass flux M, and initial cross sectional area L^2. The initial injection altitude H is defined as the distance from the level ground to the initial center of mass of the plume. The atmosphere is characterized by an ambient density ρ_o and the magnitude of the gravitational acceleration is g. Dimensionless coordinates, velocity components, and smoke density can be introduced in terms of these parameters as follows:

$$\begin{aligned} (Y,Z) &= L\,(y,z) \\ X &= (LU)^{3/2}/(gM/\rho_o)^{1/2}t \\ (V,W) &= \{gM/(\rho_o UL)\}^{1/2}(v,w) \\ \rho_p &= M/(UL^2)\rho \end{aligned} \tag{1}$$

The dimensionless horizontal (v) and vertical (w) velocities induced by the settling process, as well as the dimensionless smoke particulate density ρ are functions of the reduced transverse horizontal coordinate (y), vertical coordinate (z), and downwind coordinate (t). This nomenclature is introduced because the mathematical model of this three-dimensional steady state process is equivalent to a two dimensional time dependent process viewed in a cross-sectional plane moving downwind at the ambient wind speed U. Thus, the smoke distribution in the upwind plane $X=X_1$ in figure 17 evolves over a time interval defined by the second of eqs. (1) into the distribution at the downwind station $X=X_2$ in the figure.

The equations describing the evolution process can be written in the form:

$$\begin{aligned} &\frac{\partial\rho}{\partial t} + v\frac{\partial\rho}{\partial y} + w\frac{\partial\rho}{\partial z} = 0 \\ &\frac{\partial\omega}{\partial t} + v\frac{\partial\omega}{\partial y} + w\frac{\partial\omega}{\partial z} = -\frac{\partial\rho}{\partial y} \\ &\frac{\partial v}{\partial y} + \frac{\partial w}{\partial z} = 0 \\ &\frac{\partial w}{\partial y} - \frac{\partial v}{\partial z} = \omega \end{aligned} \tag{2}$$

The first two of equations (2) govern the evolution of the particle density and the windward component of the vorticity ω, while the last two determine the transverse velocity field at each instant in terms of ω. Equations (2) must be supplemented by initial and boundary conditions. Upwind at the injection point t=0:

$$\rho(y,z,0) = f(y,z) \tag{3}$$

$$v(y,z,0) = w(y,z,0) = 0$$

The initial particulate density distribution f(y,z) is presumed known. Since the mass flux M is specified, f(y,z) is subject to the constraint:

$$\iint dydzf(y,z) = 1 \tag{4}$$

The ground is defined by the plane z = - H/L in the present coordinate system. Since the velocities cannot penetrate the ground anywhere, the vertical velocity w must satisfy the boundary condition

$$w\ (y,-\ H/L,t) = 0 \tag{5}$$

Finally, both components of the settling induced velocities must vanish sufficiently far from the plume

$$\lim_{y,z \to \infty} (v,w) = 0 \tag{6}$$

Note that the system of equations (2)-(6), which constitute the mathematical model, depends only on the initial density distribution f(y,z) and injection altitude parameter H/L. We wish to follow the particle density downwind until most of the smoke is within some specified small distance of the ground, at which point it can be regarded as having settled out of the system. Since the primary interest is in the location of the particulate matter, the numerical method must focus on the Lagrangian coordinates of the smoke, rather than the general flow field. To this end, it is convenient to replace the continuous model of the smoke density by discrete clumps of matter s shown in figure 18. Each clump of matter carries a specific particulate mass flux and a vorticity which changes with time. The second of equations (2) shows that the vorticity is induced by horizontal density gradients, with positive gradients inducing negative vorticity as illustrated in figure 18.

The mathematical basis for this discretization is the introduction of a Lagrangian coordinate system. Each clump of matter is characterized by its initial coordinates as follows:

$$\text{at}\quad t = 0;\ y = \eta;\ z = \zeta \tag{7}$$

Then, the coordinates y, z are calculated as functions of time as solutions of the differential equations

$$\frac{\partial y}{\partial t} = v(y,z,t) \qquad \frac{\partial z}{\partial t} = w(y,z,t) \tag{8}$$

There is one pair of such equations for each clump; i.e. for each value of η,ζ. To generate the velocity fields, the evolution equations for the vorticity and density, the first two of eqs. (2), need to be rewritten in terms of the new coordinate system. The appropriate formulae are:

$$\rho = f(\eta,\zeta) \tag{9}$$

$$\frac{\partial \omega}{\partial t} = S\frac{\partial f}{\partial \zeta} - T\frac{\partial f}{\partial \eta}$$

Note that the quantity $f(\eta,\zeta)$ is the initial upwind density distribution, and that the density does not change in this system of coordinates. This is the mathematical statement of the fact that the mass flux associated with each clump is always the same as the clump progresses downwind.

The generation of the vorticity fields involves four coordinate gradients which describe the mixing and stretching of the fluid by the vortices. These quantities, denoted Q,R,S, and T are defined as follows:

$$\frac{\partial y}{\partial \eta} \equiv Q(\eta,\zeta,t) \qquad \frac{\partial y}{\partial \zeta} \equiv R(\eta,\zeta,t)$$
$$\frac{\partial z}{\partial \eta} \equiv S(\eta,\zeta,t) \qquad \frac{\partial z}{\partial \zeta} \equiv T(\eta,\zeta,t) \tag{10}$$

To preserve the intent of this method, it is important not to actually compute any spatial derivatives numerically. To avoid this, we note that <u>analytical</u> recipes for v(y,z,t) and w(y,z,t) can be generated and that these recipes can be exactly differentiated. The procedure for generating these recipes will be indicated briefly below. Given the existence of such expressions, however, it is easy to generate evolution equations for Q,R,S, and T. The necessary equations are:

$$\frac{\partial Q}{\partial t} = Q \frac{\partial v}{\partial y} + S \frac{\partial v}{\partial z}$$
$$\frac{\partial R}{\partial t} = R \frac{\partial v}{\partial y} + T \frac{\partial v}{\partial z} \tag{11}$$
$$\frac{\partial S}{\partial t} = Q \frac{\partial w}{\partial y} + S \frac{\partial w}{\partial z}$$
$$\frac{\partial T}{\partial t} = R \frac{\partial w}{\partial y} + T \frac{\partial w}{\partial z}$$

Equations (8), (9), and (11) constitute a set of seven ordinary differential equations and one algebraic statement that must be solved to describe the evolution of each clump. They are equivalent to solving equations (2) everywhere in space. Obviously, any method which attempts to solve the equations everywhere is going to yield a much cruder approximation to the quantities of interest then one which concentrates attention directly on the desired information. Thus, it is worthwhile to expend this much effort on tracking the fate of a single clump of particulate matter, if <u>no</u> resources have to be devoted to calculating quantities outside the smoke cloud.

The final piece of information required to implement this method is the explicit representation of the velocities in terms of the coordinates y,z. To this end, it is convenient to introduce a stream function $\Psi(y,z,t)$ that satisfies the third of eqs. (2) identically.

$$\frac{\partial \Psi}{\partial z} = v; \quad \frac{\partial \Psi}{\partial y} = - w \tag{12}$$

Substitution of eqs. (12) into the last of eqs. (2) yields a Poisson equation for Ψ in terms of ω. The solution can be expressed in terms of a Greens function $G(y,z,y_o,z_o)$ as:

$$\Psi = \iint dy_o dz_o \; G(y,z,y_o z_o) \; \omega(y_o,z_o t)$$

$$G = -\frac{1}{2\pi}\left\{ \log (r_+) - \log (r_-) - \log (rI_-) + \log (rI_+) \right\}$$

$$(r_+)^2 = (y-y_o)^2 + (z-z_o)^2$$

$$(r_-)^2 = (y+y_o)^2 + (z-z_o)^2 \qquad (13)$$

$$(rI_-)^2 = (y-y_o)^2 + \{z + [2(H/L) + z_o]\}^2$$

$$(rI_+)^2 = (y+y_o)^2 + \{z + [2(H/L) + z_o]\}^2$$

Physically, the Greens function represents the flow induced by the vortex pair associated with two clumps as shown in figure 19a. The signs of the vortices are such that the direction of the swirling motion, as indicated by the arrows, induces a downward flow. This accounts for the first two terms in the expression for G. The last two terms account for the image vortices shown in figure 19b generated by the presence of the ground. They induce the swirling motions shown by the arrows which tend to push the clumps of particulate outward as they near the ground.

The numerical simulation will require the simultaneous tracking of a few thousand clumps of material to adequately represent the turbulent mixing generated by the settling process. Numerical methods of this kind to simulate processes quite analogues to the one of interest here have been pioneered by Ghoniem [17], who has demonstrated their ability to predict overall characteristics of turbulent flows. The approach taken here is more specialized than his, and will hopefully yield more accurate results for the particular problem with which we are concerned.

5.0 CONCLUSIONS

Increasing oil surface temperature and smoke production during the burning of a crude oil pool fire are evidence that lower boiling temperature fractions are consumed preferentially during the early part of the burn.

The smoke production during boiling of the supporting water layer is reduced by up to a factor of five when compared to that with no boiling. The smoke yield decreases by more than a factor of two as the oil layer thickness is decreased from 10 mm to 2 mm. The smaller yield for the thin oil layer results from boiling in the water layer occurring over most of the burn.

The total PAH contained in the oil residue and the smoke and vapors produced by combustion is less than that contained in the original oil. The crude oil and the residue which is left on the water have the same relative concentration of the various PAH compounds measured on a per unit mass of original oil basis. However, the concentration of PAHs with 5 or more rings, which includes benzo[a]pyrene, is 10 to 20 times greater in the smoke compared to the fuel. While about 90% of the PAHs for the oil and residue have three rings, the PAH content of the smoke/vapor is equally divided among three rings, four rings, and 5 or more rings.

As the PAH concentrations for the Alberta Sweet crude oil and the burn residue

were found to be very similar, it might be possible to use the PAH distribution in the burn residue to identify the crude oil that was burned.

Particle agglomeration for Alberta Sweet crude oil smoke measured in the aging/dilution chamber over 90 minutes (corresponding to approximately one day in an actual fire plume) leads to a 30% increase in aerodynamic particle size.

6.0 ACKNOWLEDGEMENTS

This work was supported by the Minerals Management Service, U.S. Department of the Interior. Special technical assistance and cooperation in chemical analysis was provided by Conservation and Protection Service, Environment Canada. Special thanks is extended to Mr. Ed Tennyson and Mr. John Gregory who organized and consulted in the development of this research program. Dr. M. F. Fingas was especially helpful in consultations about the chemical analysis of the crude oil, residue and smoke samples. Mr. N. Bryner was responsible for the construction and operation of the smoke aging/dilution chamber and for the collection of the smoke particulate. The assistance of Dr. Benner and Dr. Wise was indispensible in the analysis for PAH compounds. The oil level control device was designed, assembled and made operational by Mr. J.S. Steel, who also provided technical advice on instrumentation. Dr. K.M. Tu made the critical oil level control adjustments and also performed the radiometer calibrations. Essential support in assembling and maintaining the test instrumentation and in the collection of test data was provided by R. Zile, M.E. Womble, R. McLane and G. Roadarmel.

7.0 REFERENCES

1. Evans, D., Mulholland, G., Gross, D., and Baum, H., Saito K., "Environmental Effects of Oil Spill Combustion," NISTIR 88-3822 U.S. Department of Commerce, National Institute of Standards and Technology, Gaithersburg, MD 20899, (1988).

2. Petty, S. E.,Combustion of Crude Oil on Water, Fire Safety Journal, 5, 123-134, (1983).

3. Burgoyne, J. H., and Katan, L. L., Fires in Open Tanks of Petroleum Products: Some Fundamental Aspects, J. Inst. Petr., 33, No.279, (1947).

4. Blinov, V. I. and Khudyakov, G. N., Diffusion Burning of Liquids, Moscow Academy of Sciences, 1961, U.S. Army Research and Development Laboratories Translation T-1490a-c (1963).

5. Hottel, H. C., Fire Research Abstracts and Reviews, 1, No 2, (1959).

6. Johnson, R. L., Shah, J. J., Cary, R. A., and Huntzicker, J. J., " An Automated Thermal-Optical Method for the Analysis of Carbonaceous Aerosol," in ACS Symposium Series, No. 167, Atmospheric Aerosol: Source/Air Quality Relationships, ed. by E. S. Macias and P. K. Hopke, (1981).

7. Wise, S. A., Benner, B. A., Chesler, S. N., Hilpert, L. R., Vogt, C. R., and May, W. E., "Characterization of the Polycyclic Aromatic Hydrocarbons from Two Standard Reference Material Air Particulate Samples," Anal. Chem., 58, 3068, (1986).

8. Reference Bjorseth, A. (ed.), Handbook of Polycyclic Aromatic Hydrocarbons, Marcel Dekker Inc., New York.

9. The Consumption and Expenditures, April 1984 to March 1985, Energy Information Administration, U.S. Department of Energy, 1985.

10. Cashdollar, K.L., Lee, C.K., and Singer, J.M., "Three-Wavelength Light Transmission Technique to Measure Smoke Particle Size and Concentration," Applied Optics, 18, 1763-1769 (1979).

11. Dryer, F. L., "Water Addition to Practical Combustion Systems-Concepts and Applications," Sixteenth Symposium (International) on Combustion, The Combustion Institute, Pittsburgh, 279-295 (1982).

12. Schug, K. P., Manheimer-Timnat, Y., Yaccarino, P., and Glassman, I., "Sooting Behavior of Gaseous Hydrocarbon Diffusion Flames and the Influence of Additives," Combustion Science and Technology, 22, 235-250 (1980).

13. Rao, V. K. and Bardon, M. F., The Effect of Water on Gas Phase Soot Formation in Laminar Diffusion Flames, Combustion and Flame, 55, 73-78 (1984).

14. Longwell, J. P., "Polycyclic Aromatic Hydrocarbons and Soot from Practical Combustion Systems, Soot in Combustion Systems and its Toxic Properties, ed. by J. Lahaye and G. Prado, Plenum Press, New York, 38 (1981).

15. Evans, D., Baum, H., McCaffrey, B., Mulholland, G., Harkleroad, M., and Manders, W., Combustion of Oil on Water, NBSIR 86-3420, U.S. Department of Commerce, National Bureau of Standards, Gaithersburg, MD 20899, (1987).

16. Mulholland, G. W., Bryner, N. P., Ives, L. K., Rogers, C. F., Hudson, J. G., and Hallett, J., "Effect of Cloud Processing on the Optical Properties of Smoke," submitted to Nature.

17. Ghoniem, A. F., Heidarinejad, G., and Krishnan, A., On Mixing, Baroclinicity, and the Effect of Strain in a Chemically - Reacting Shear Layer, AIAA 26th Aerospace Sciences Meeting, Paper AIAA-88-0729, Jan.11-14, 1988.

Table 1. Summary of Measured Burning Data in 1.2 m Diameter Pan

Test	Oil Layer Thickness	Wt	Max Flame Temp	Max RHR	Maximum Radiation Feedback ctr	rim	Maximum External Radiation	Burning Rate[c]	Burn Time	Initial Water Temp	Oil Residue
	mm	kg	°C	MW/m^2	kW/m^2		kW/m^2	mm/min	min	°C	kg
A05	10	9.36	900	2.2	53	39	11	2.4	4.00	10	1.10
A06	10	9.36	900	2.3	76	22	13	2.3	4.33	15	1.01
A07	10	9.36	880	1.6	81	21	9.2	2.2	4.47	28	1.32
A08	10	9.36	890	1.6	74	27	9.8	2.0	5.30	5	0.92
T01	5	5.00	850	1.5	23	14	9.2	2.4	2.2	8	0.14
T02	10	9.76	890	1.8	32	14	10	3.2	3.2	15	0.10
A09[a]	5	4.68	290	1.4	48	19	19	4.0	1.77	16	0.86
A10[a]	10	9.36	390	2.2	45	22	21	4.0	2.57	18	1.03
A11[b]	10	9.36	460	1.9	42	16	21	2.9	3.0	20	1.18
D01	10	8.20	960	2.3	54	31	12	4.5	4.0	2	0.06
A12	10	9.36	890	2.5	66	21	12	1.6-4.8[d]	3.60	5	0.84
T03	10	9.76	870	1.7	23	21	11	3.7	3.2	6	0.08
A13	10	9.36	890	2.6	60	26	12	1.7-4.8[d]	3.9	10	0.92

[a] Applied wind velocity 2.5 m/s
[b] Applied wind velocity 1.0 m/s
[c] Burning rate estimated from the volume flow rate of water supplied to maintain the burning surface at a constant level.
[d] Individual values for steady burning and vigorous boiling periods

Table 2. Properties of Test Liquids (Typical)

Liquid	Grade (Purity) (%)	Boiling Point	Density @ 20°C	Flash Point	Heat Capac[a] @ mean temp	Thermal Conductivity[a]		Heat of Vaporiz'n[a] @20°C	@b.p.	Net Heat of Comb.[a]
		°C	kg/m^3	°C	kJ/kgK	W/mK		kJ/kg		MJ/kg
Alberta Sweet		37-350+	840	7	2.34[b]	0.120	0.0874		305[b]	43.4[b]
n-Decane	Techn'l (99)	174	730	44	2.50	0.130	0.0829	354	276	44.2
Toluene	ACS (99)	111	860	5	1.88	0.135	0.110	409	360	40.5

[a] For pure toluene, and n-decane, values of k_{20}, k_{bp}, C_p, H_v and H_c are based on data and methods in Technical Data Book - Petroleum Refining, Metric Edition 1977, 1984. For Alberta Sweet crude, k_{bp} is based on laboratory measurements at 20°C and analogous extrapolation techniques at an approximate boiling point of 250°C.

[b] Computed on the basis of mass fraction for a simulated blend representing Alberta Sweet crude (Table 4).

Table 3. Energy Balance Estimates for the Steady Burning Period

Test	Liquid	Test Period	Q_i Incident Radiant Energy ctr	Q_i Incident Radiant Energy rim	Burning Rate	Q_v Energy Req'd for Vaporization	Surface Temp Gradient	Q_c Heat Conduction Into Oil
		sec	kW/m^2	kW/m^2	mm/min	kW/m^2	°C/mm	kW/m^2
A12	Alberta Sweet	30-125	40-65	18	1.6	6.7	29	2.5
D01	n-Decane	60-150	34	27	4.5	15.1	28	2.3
T03	Toluene	60-150	19	14	3.7	19.1	30	3.3

Table 4. Composition and Properties of Simulated Crude Oil

Component		Assumed Mass Fraction	Density @ 20°C kg/m^3	Boiling Point °C	Heat of Vaporization @ Boiling Pt kJ/kg	Net Heat of Combustion MJ/kg
C_5H_{12}	Pentane	0.10	626	36	357.2	44.98
$C_{10}H_{20}$	Cyclodecane	0.75	858	202	286.4	43.82
C_7H_8	Toluene	0.15	867	111	360.2	40.53

Source: Technical Data Book - Petroleum Refining, Metric Edition 1977, 1984

Table 5. Comparison of Alberta Sweet Crude Oil Burning Data for 0.6 m and 1.2 m Diameter Pans

Oil Layer Thickness mm	Pan Dia. m	Heat Release Rate, MW/m^2 Steady	Heat Release Rate, MW/m^2 Peak	Burning Rate, g/m^2s Steady	Burning Rate, g/m^2s Peak	% Oil Burned	Time to Boilover s	Effective Heat of Combustion MJ/kg	Burn Time s
2	0.6	-	0.7	-	18	54	35	35	82
2	1.2	-	0.9	-		67			
3	0.6	-	1.1	-	32	73	38	33	99
5	0.6	0.60	1.9	15	38	76	100	36	151
5	1.2	0.89	1.9	-	-	86	55		
10	0.6	0.67	2.9	15	83	83	271	42	310
10	1.2	1.00	2.5	22	67	92	130		

Table 6. Effect of Layer Thickness on Smoke Emission from Alberta Sweet Crude Oil (60 cm diameter pan)

Oil Layer Thickness mm	Average Burning Rate g/s	Smoke Yield g/g	k m^{-1}	σ_f m^2/g	σ_s m^2/g
2	2.2	0.035	0.4	0.33	9
3	3.9	0.050	1.0	0.48	7
5	5.6	0.080	1.4	0.51	7
10	5.3	0.080	1.7	0.65	8
30[a]	5.1	0.100		0.88	9.4

[a] The mass loss and smoke measurements correspond to the steady burning phase.

Table 7. Concentration of PAH in Alberta Sweet Crude Oil and its Burn Residue

PAH	μg PAH/g sample Crude oil "Q"	Crude oil "S"	Residue "D" 2 mm layer	Residue "Z" 5 mm layer	Residue "Y" 10 mm layer
Acenaphthylene	13		54	26	
Acenaphthene	57		15	10	
Fluorene	59		47	35	
2-Methyl fluorene	150		110	160	
Phenanthrene	150	147	140	130	120
Methylphenanthrene	-	371	-	-	330
Dimethylphenanthrene	-	497	-	-	520
Anthracene	11		19	13	
Fluoranthene	6		22	11	
Pyrene	17		30	25	
1-Methyl Pyrene	39		16	19	
Benzo[ghi]fluoranthene	-		1	2	
Chrysene/Triphenylene	30		24	34	
Benzo[b]fluoranthene	4		7	2	
Benzo[e]pyrene	5		6	6	
Benzo[a]pyrene	-		4	3	
2-Methyl cholanthrene	3		3	3	
Benzo[ghi]perylene	-		2	-	
Total PAH	540	1020	500	480	970

[1] Samples S and Y were analyzed at the National Institute of Standards and Technology and samples D, K, and Q were analyzed at Environment Canada.

Table 8. Concentrations of Six PAHs Collected in the Vapor and Particulate Phases from the Combustion of Alberta Sweet Crude Oil

Sample		μg in extract					
		Acenaphthylene	Phenanthrene	Anthracene	Fluoranthene	Acephenanthrylene	Pyrene
7	2 mm layer						
	T-07[1]	-	1.5	0.4	2.5	-	2.9
	PU-07[2]	13.0	8.9	2.3	1.8	-	1.6
	% in vapor	100	86	85	41	-	35
9	3 mm layer						
	T-09	-	3.2	0.7	4.9	3.0	6.2
	PU-09	-	12.6	3.0	2.3	1.0	2.2
	% in vapor	-	80	82	32	24	26
12	5 mm layer						
	T-12	-	3.3	1.0	4.3	2.5	5.2
	PU-12	-	4.7	1.0	0.5	0.2	0.5
	% in vapor	-	59	50	11	8	9
5	10 mm layer						
	T-05	-	9.0	2.7	9.4	5.3	10.6
	PU-05	-	10.2	2.0	0.2	0.1	0.2
	% in vapor	-	53	43	2	1	2
6	10 mm layer						
	T-06	-	7.2	2.5	9.7	-	9.8
	PU-06	25.3	11.1	3.1	0.3	-	0.3
	% in vapor	100	61	56	3	-	3

[1] Teflon filter samples (particulate phase). Samples 5, 9, and 12 were analyzed at the National Institute of Standards and Technology and samples 6 and 7 at Environment Canada.
[2] Polyurethane foam samples (vapor phase).

Table 9. Concentration of PAH (Vapor and Particulate) Produced by the Combustion of Alberta Sweet Crude Oil

PAH	μg PAH/g soot[1]				
	2 mm, T-07 & PU-07	3 mm, T-09 & PU-09	5 mm, T-12 & PU-12	10 mm, T-05 & PU-05	30 mm, C-5[2] #1
Acenaphthylene	1740	-	-	-	-
Phenanthrene	1400	1610	910	1820	910
Anthracene	360	400	210	440	260
Methylphenanthrene	-	49	100	110	-
Fluoranthene	580	770	590	950	700
Acephenanthrylene	-	410	330	520	380
Pyrene	610	890	680	1070	900
Benzo[a]fluorene	70	-	-	-	-
Benzo[b]fluorene	70	-	-	-	-
1-Methyl pyrene	56	-	-	-	-
Benz[a]anthracene	155	200	160	260	220
Chrysene/Triphenylene	78	230	170	260	220
Benzo[b,j+k]fluoranthene	-	370	260	430	380
Benzo[a]fluoranthene	-	120	81	130	-
Benzo[b]fluoranthene	410	-	-	-	-
Benzo[ghi]fluoranthene	160	-	-	-	-
Benzo[e]pyrene	110	120	90	140	120
Benzo[a]pyrene	230	260	190	310	240
Perylene	56	19	35	5	42
Indeno[1,2,3-cd]pyrene	200	180	120	200	190
Benzo[ghi]perylene	120	220	160	250	210
Coronene		250	45	190	-
Total PAH	4670(6410[3])	6100	4130	7090	4770

[1] Uncertainties estimated to be about ± 10% of the tabulated concentration.
[2] These results are taken from the 1987 report [1] based on sample collected during steady burning before boilover.
[3] The value in parentheses includes acenaphthylene.

Table 10. Comparison of PAH Content of Crude Oil, Oil Residue, and Smoke (Vapor and Particulate) per Gram of Fuel Consumed

Sample/layer thickness	μg PAH/g crude oil						
	3 rings	3 rings/ methyl	4 rings	4 rings/ methyl	5 or more	5 or more rings/methyl	Total
ALBERTA SWEET	290	1020	53	39	9	3	1440
Residue							
2 mm	120	470	35	7	10	1	640
3 mm							380[1]
5 mm	50	240	17	5	4	1	320
10 mm							230[1]
Smoke[2]							
2 mm	62(120)[3]	2	69	2	71	-	210(330)
3 mm	100(190)	2	130	3	110	-	350(440)
5 mm	90(230)	8	170	4	120	-	390(530)
10 mm	180(320)	8	260	4	180	-	630(770)

[1] The overall estimates for the 3 mm and 10 mm layers are based on the results for the 2 mm and 5 mm layers and the measured residue fraction.

[2] In computing the results using Table 9 the missing PAH values such as benzo[a]fluoranthene for the 2 mm layer thickness are estimated based on related entries in Table 9. (the 3 mm test in the case of benzo[a]fluoranthene)

[3] The values in parentheses include acenaphthylene.

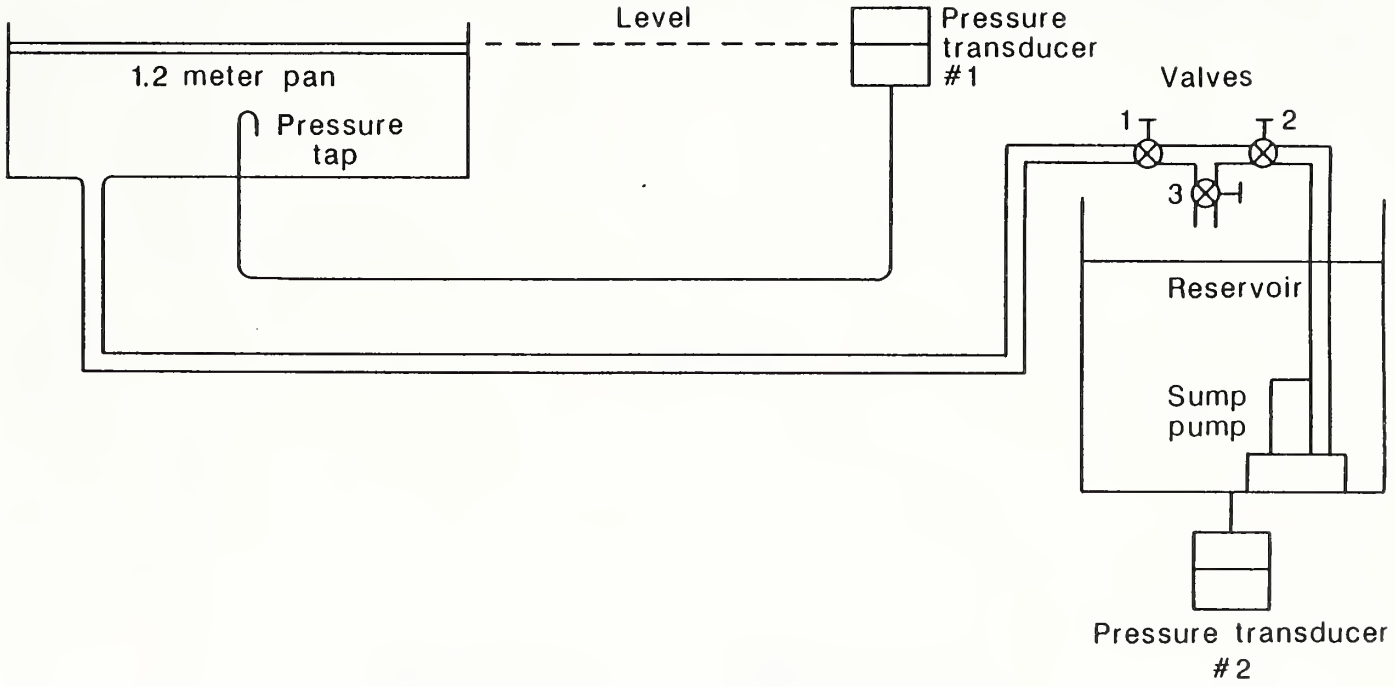

Figure 1. Schematic diagram of the fuel level control device

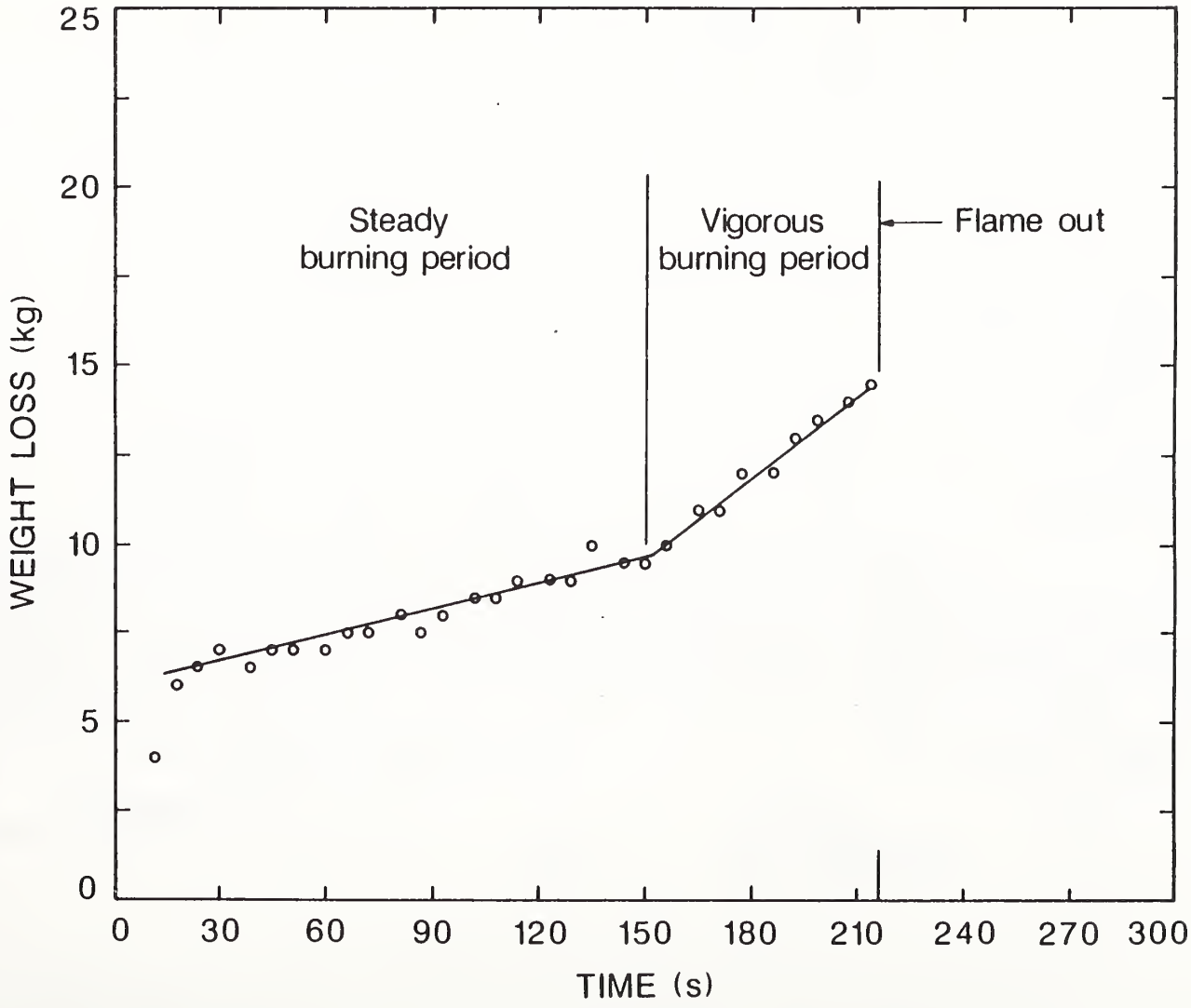

Figure 2. Recorded Weight of Water Supplied to maintain oil level (Test A12)

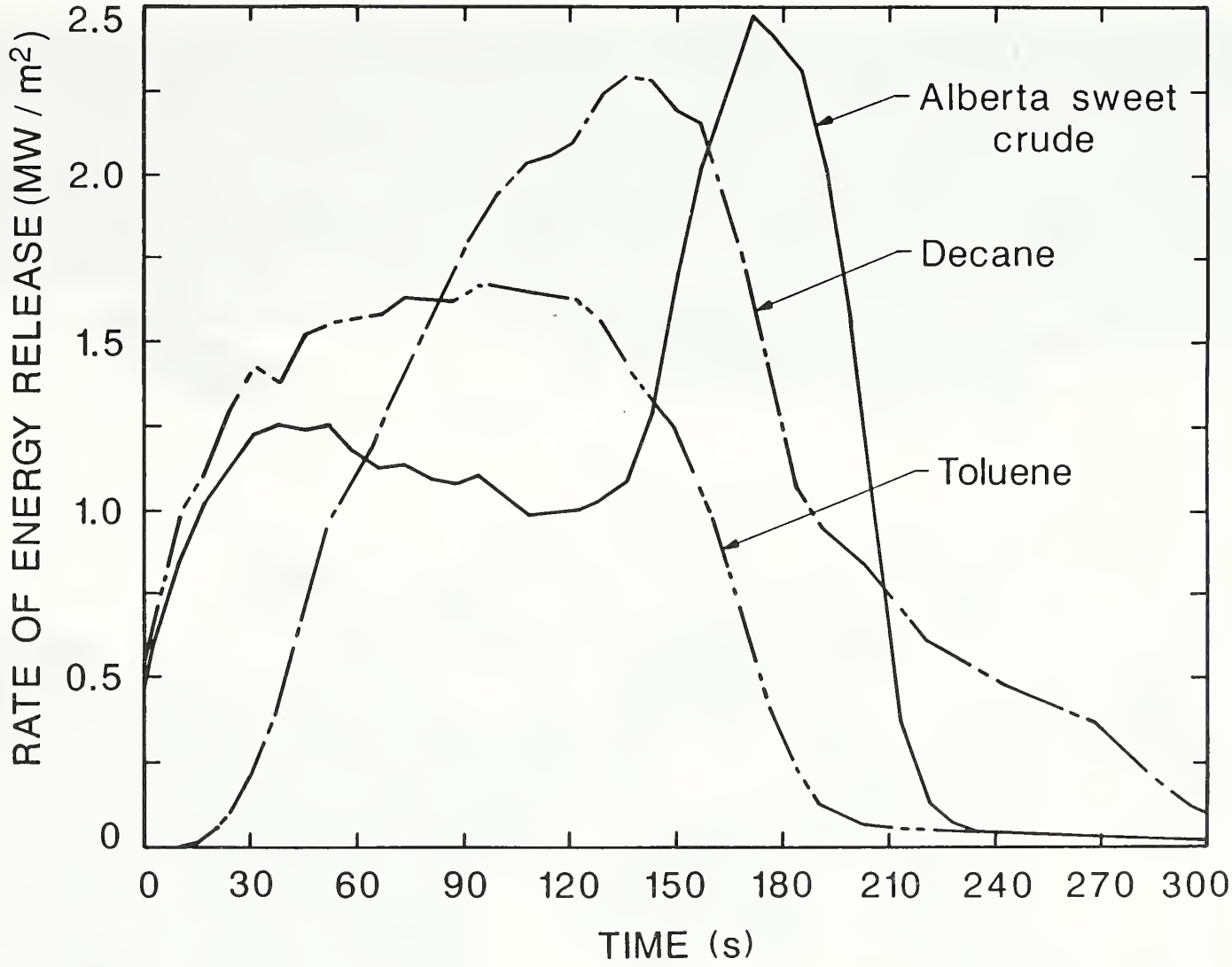

Figure 3. Energy release rate per square meter for Alberta Sweet crude oil and pure hydrocarbons, tests A12, D01, T03 (10 mm layer thickness, fuel area 1.13 m^2)

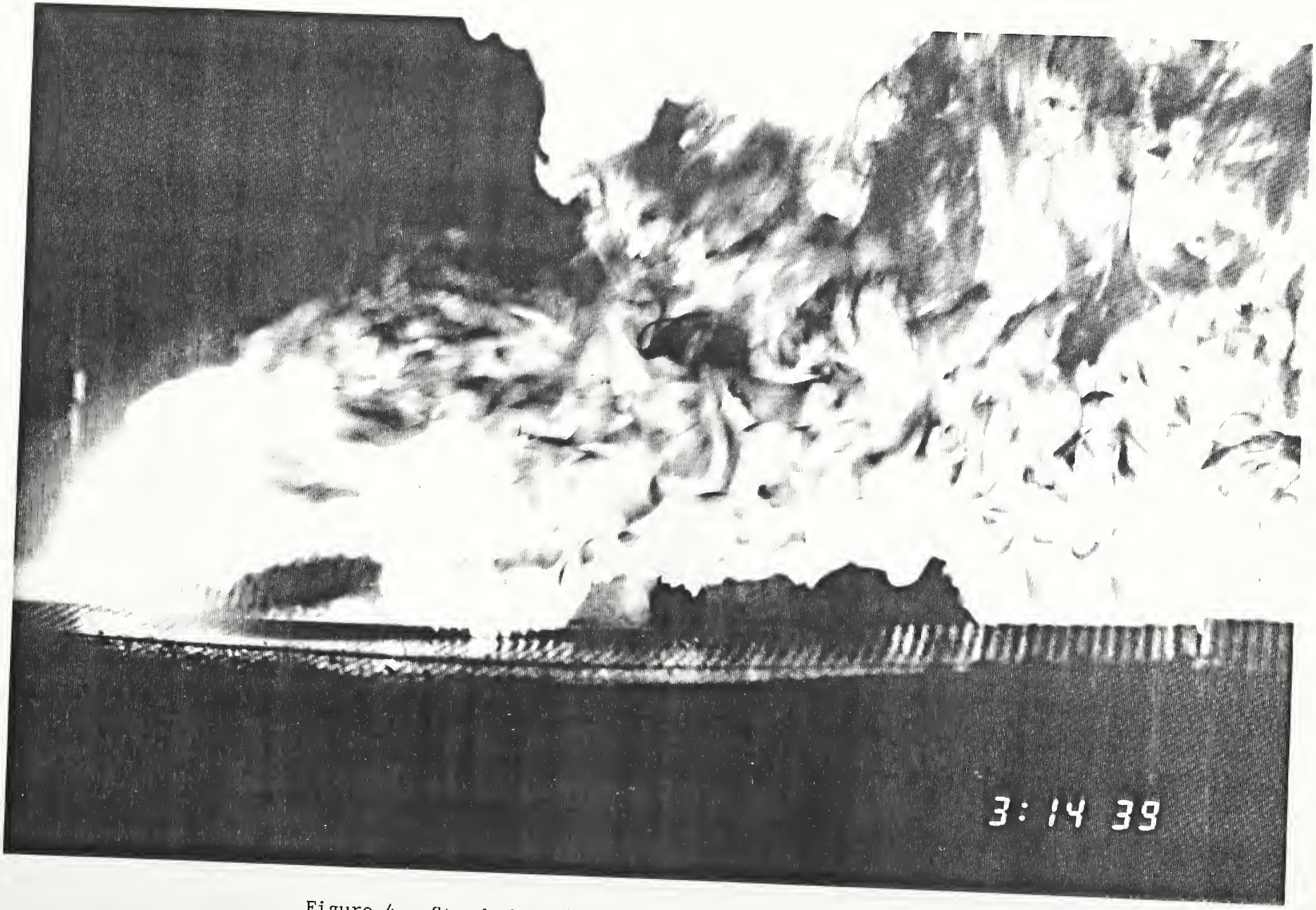

Figure 4. Steady burning of toluene showing flame lifting

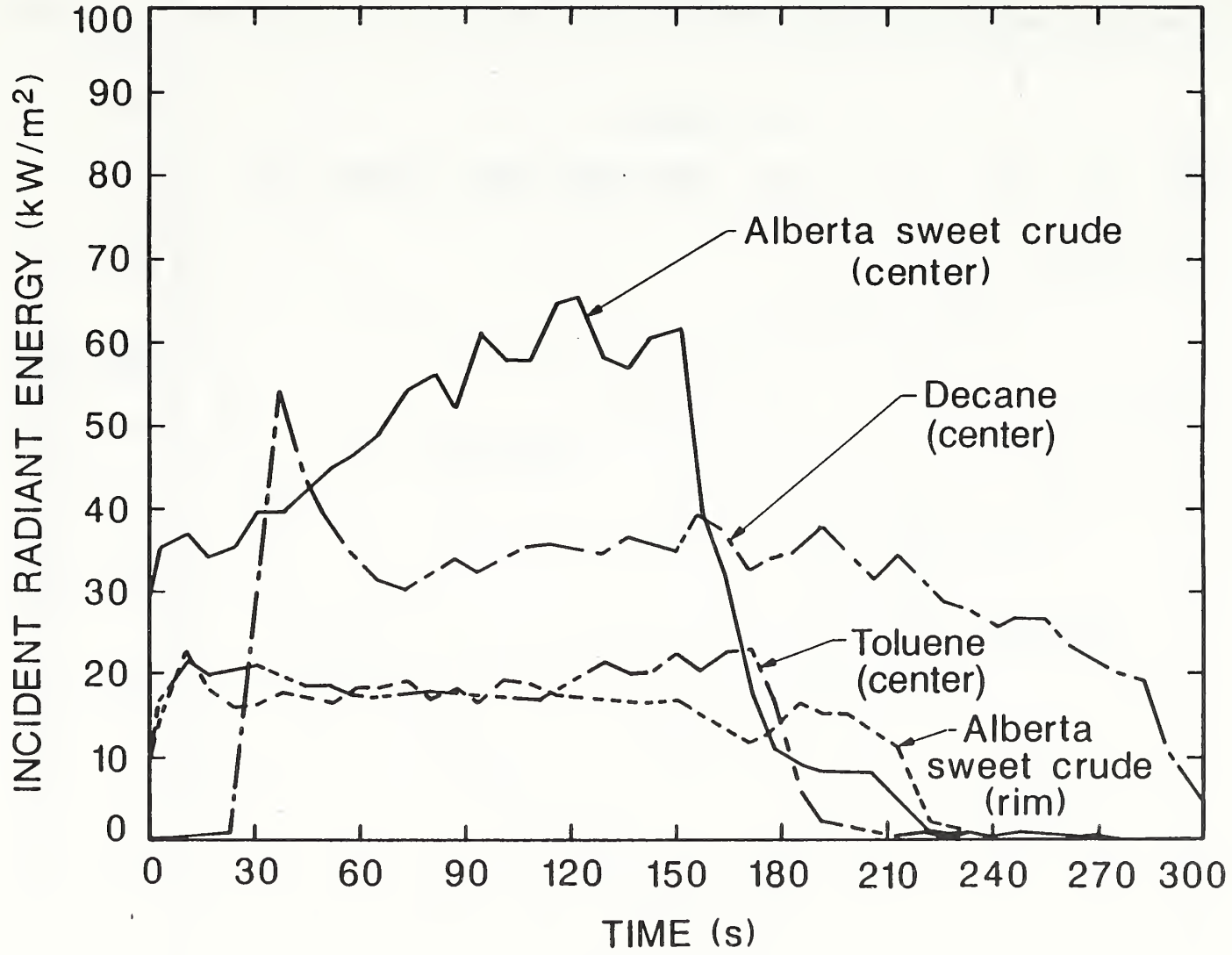

Figure 5. Radiant energy feedback to the fuel surface for Alberta Sweet hydrocarbons, tests A12, D01, T03 (10 mm layer thickness, fuel area 1.13 m^2)

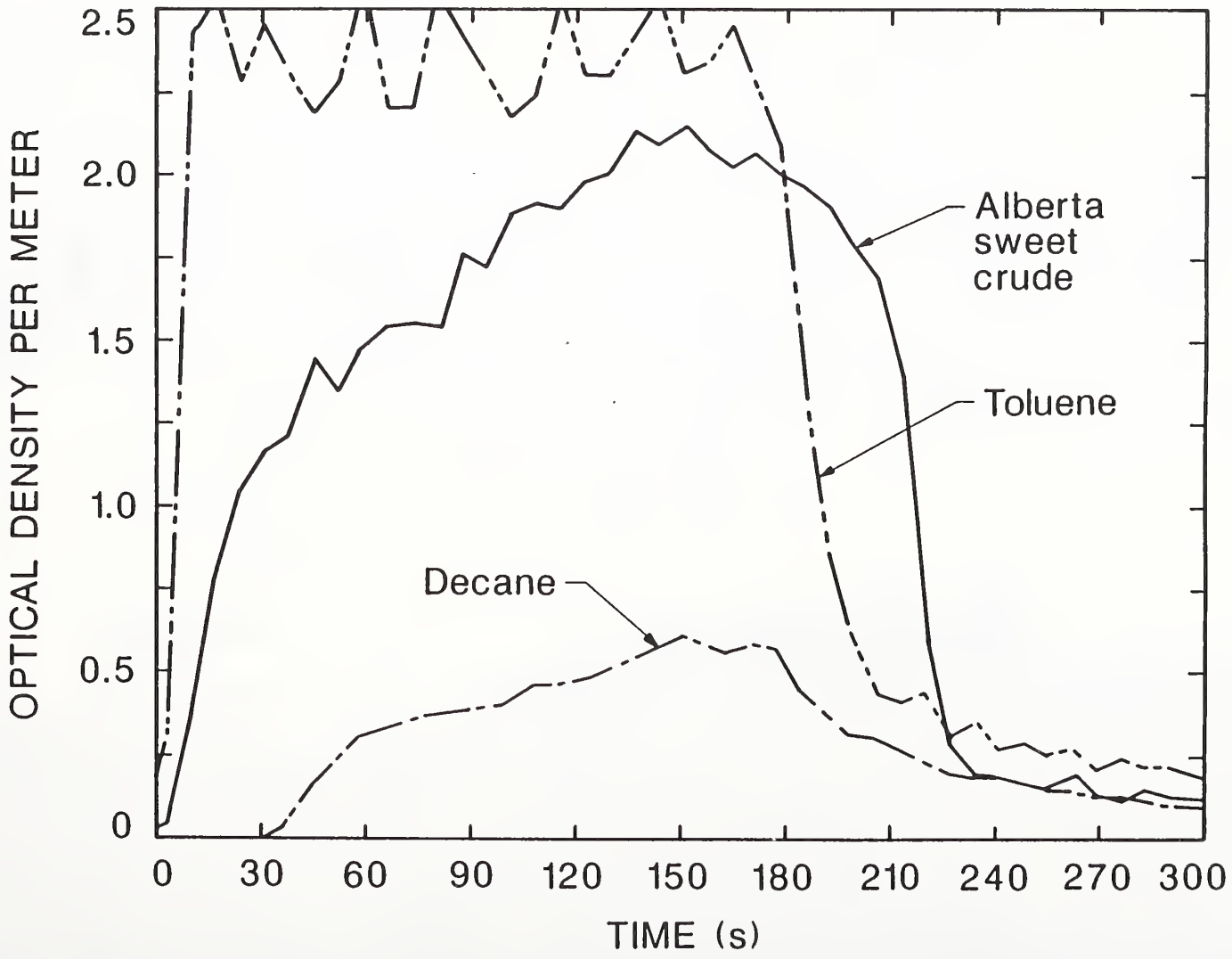

Figure 6. Smoke obscuration in stack for Alberta Sweet crude oil and pure hydrocarbons, tests A12, D01, T03 (10 mm layer thickness, fuel area 1.13 m^2)

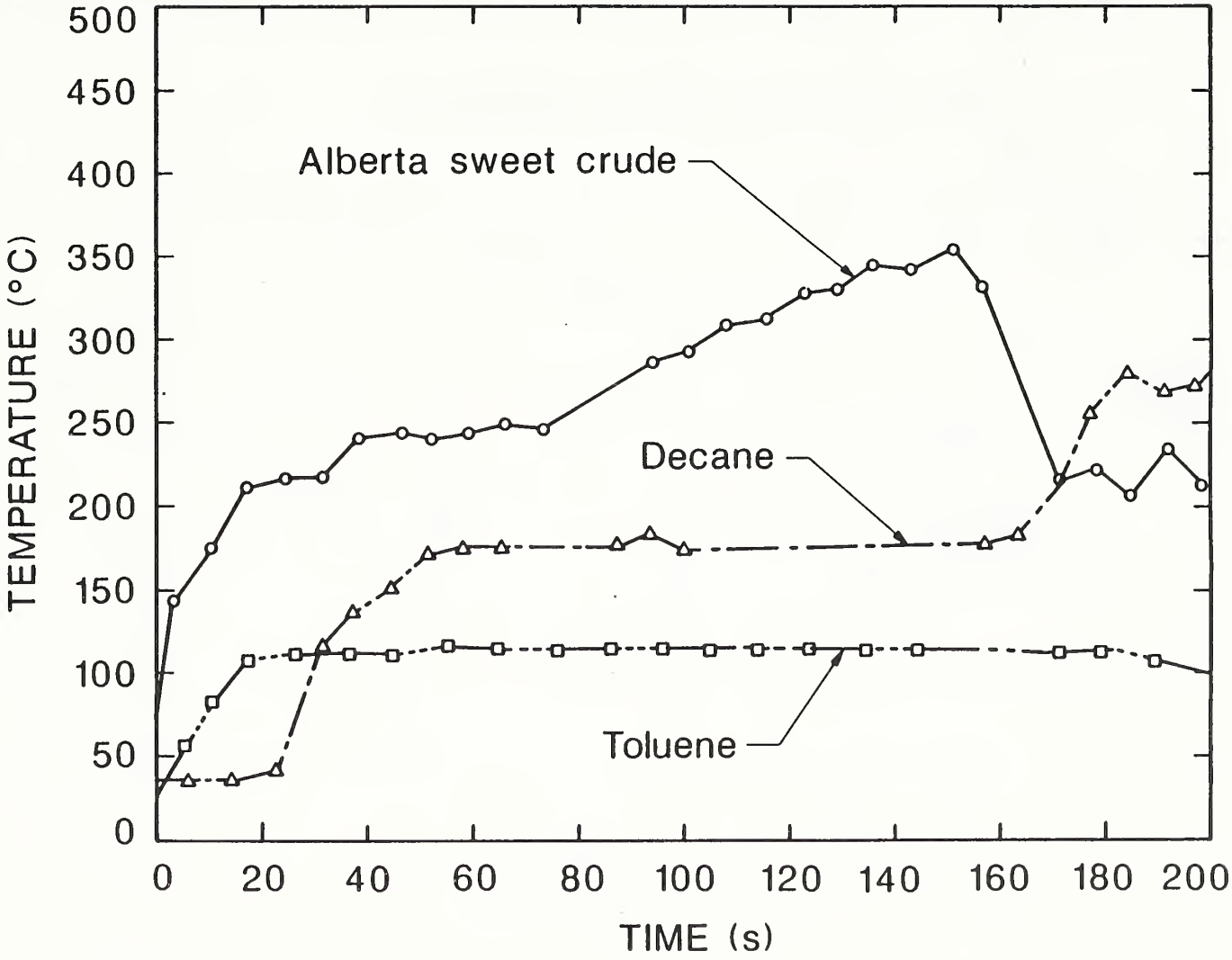

Figure 7. Oil surface temperature at rim for Alberta Sweet crude oil and pure hydrocarbons, tests A12, D01, T03 (10 mm layer thickness, fuel area 1.13 m^2)

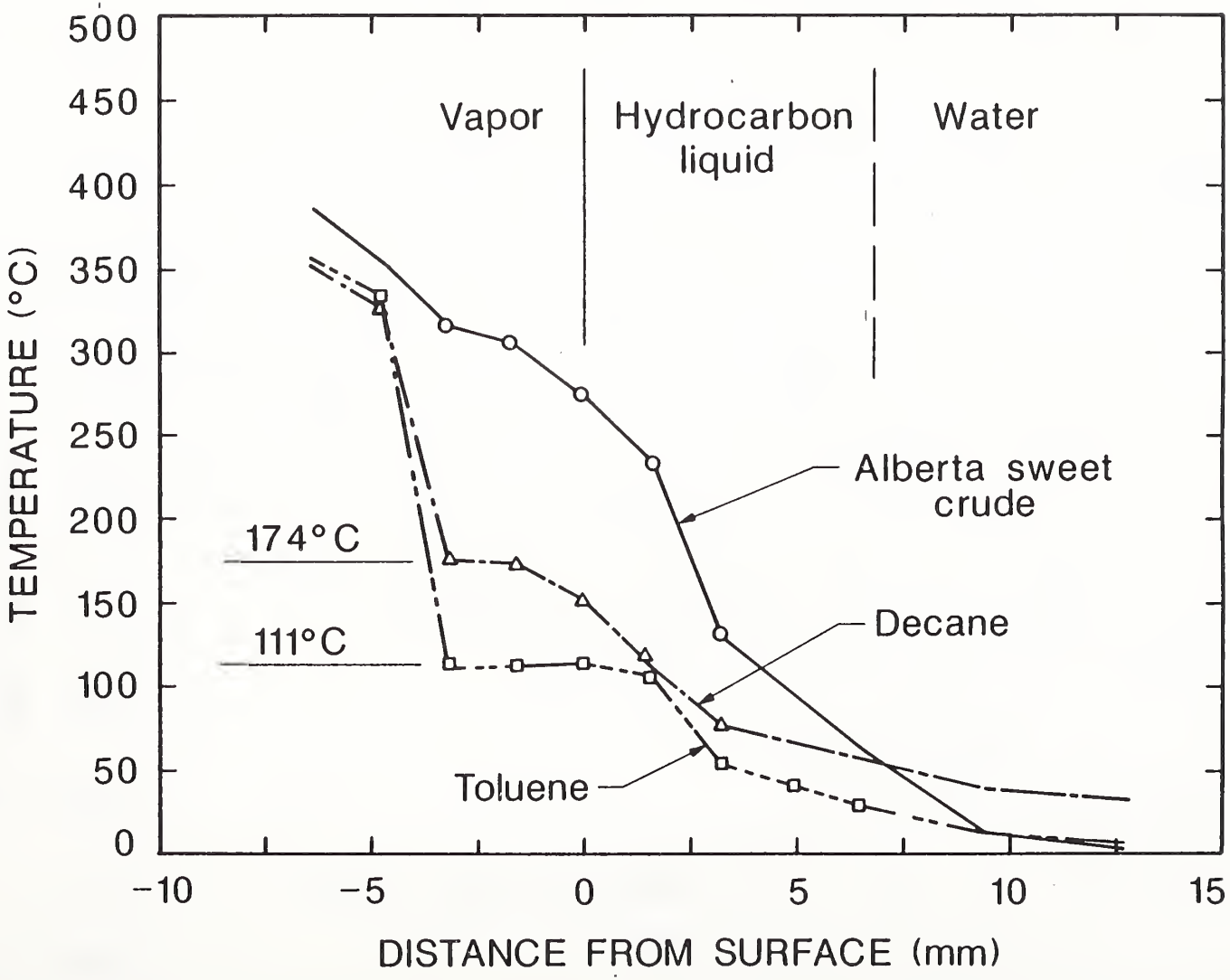

Figure 8. Temperature profile at center of pan (t=115 seconds), for Alberta Sweet crude oil and pure hydrocarbons tests A12, D01, T03 (10 mm layer thickness, fuel area 1.13 m^2)

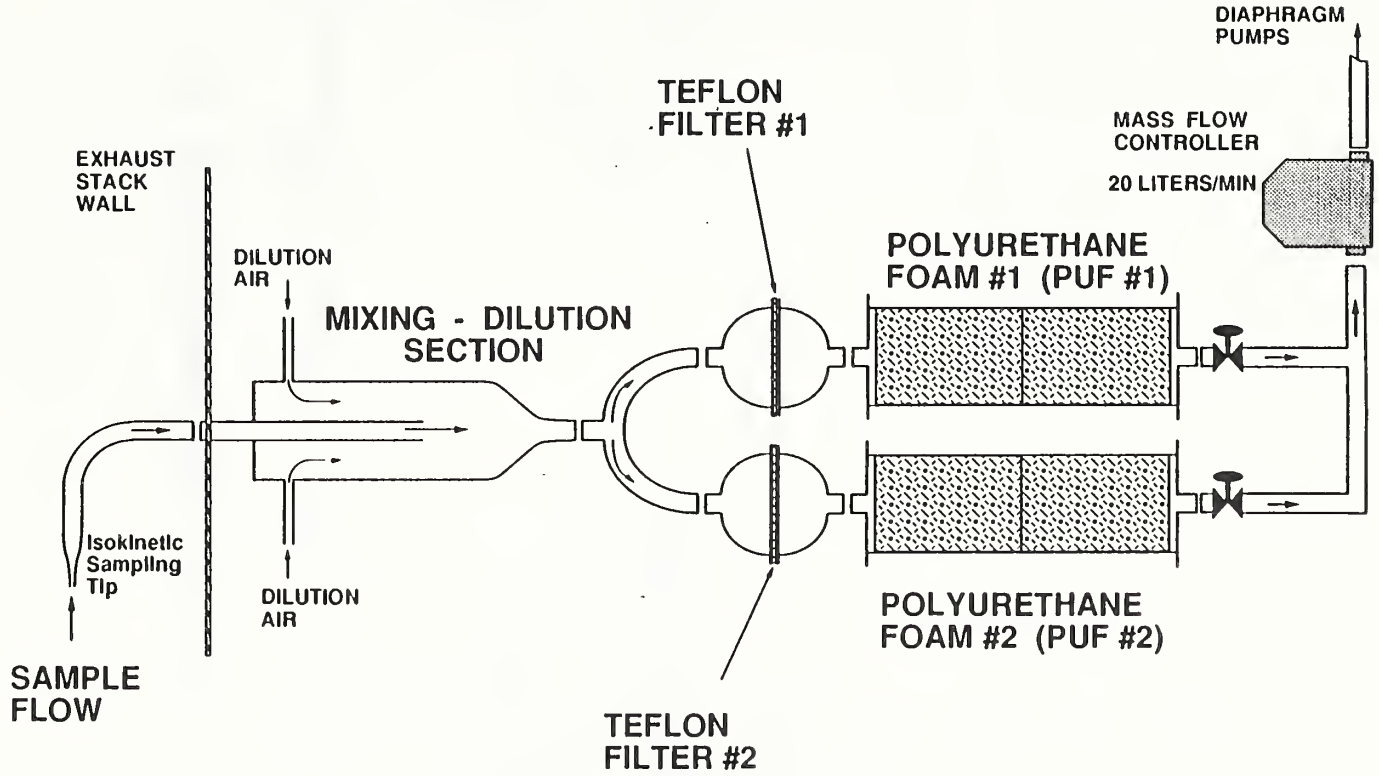

Figure 9. Smoke/PAH sample collection system

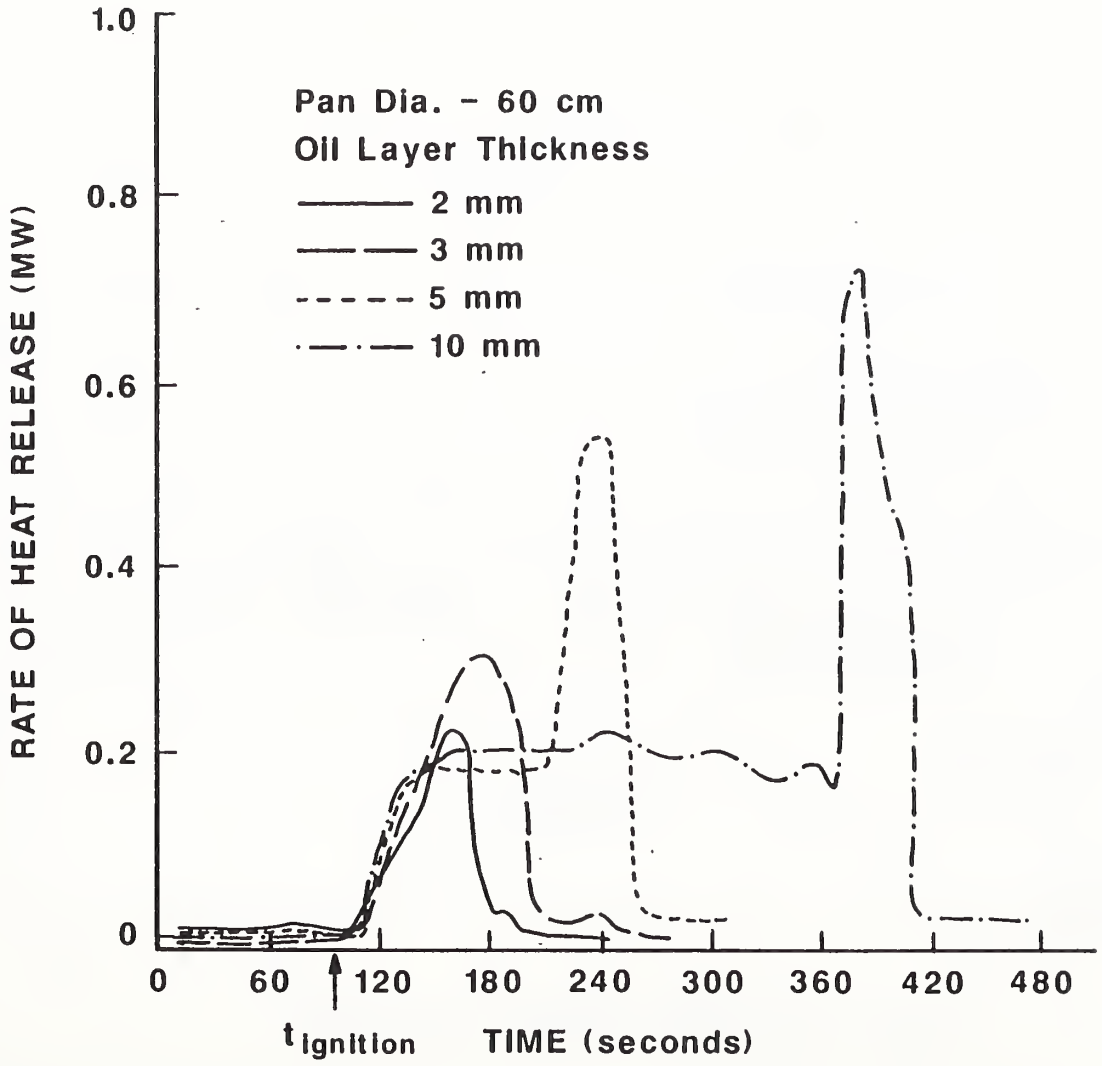

Figure 10. Effect of oil layer thickness on energy release rate for crude oil fires

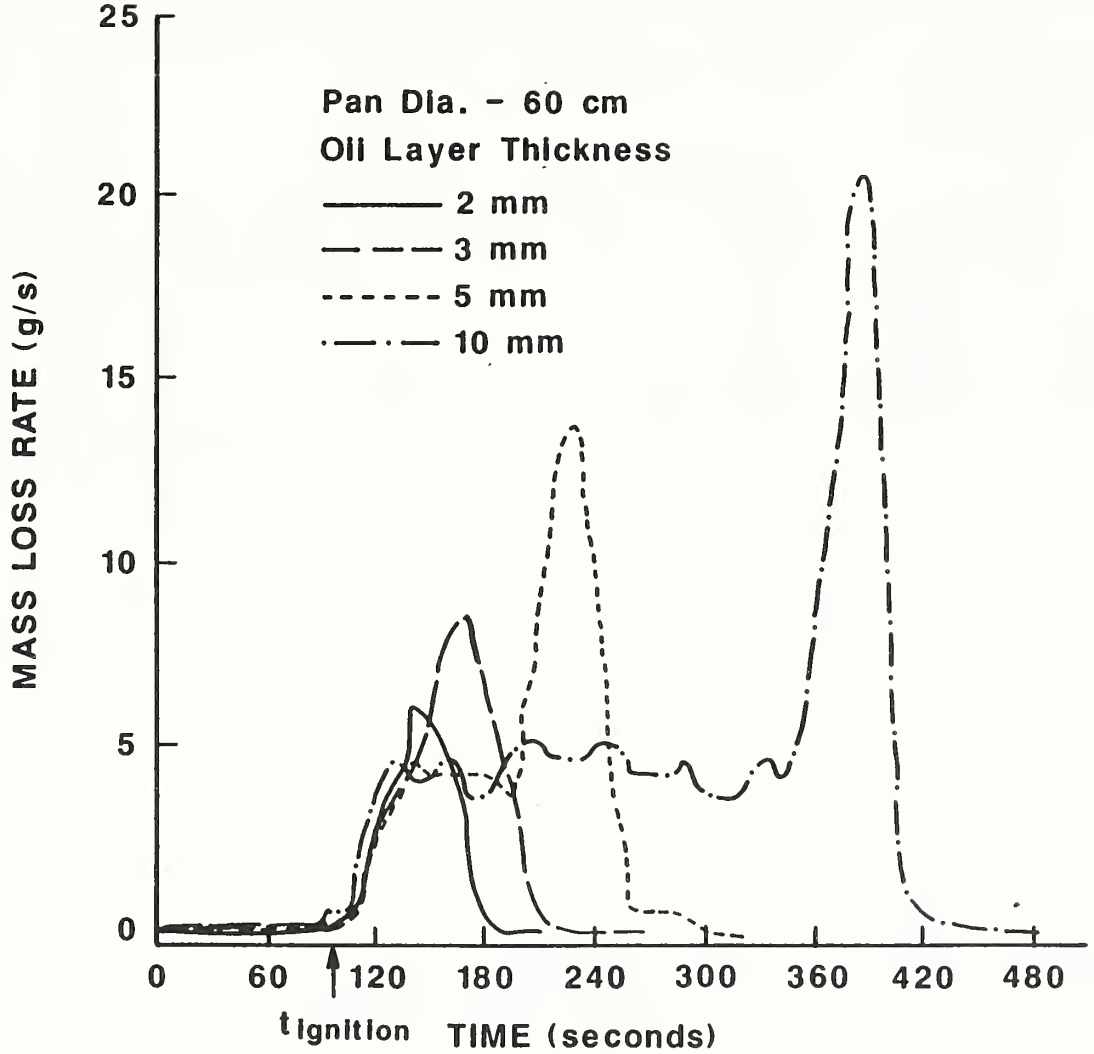

Figure 11. Effect of oil layer thickness on mass loss rate (fuel) for crude oil fires

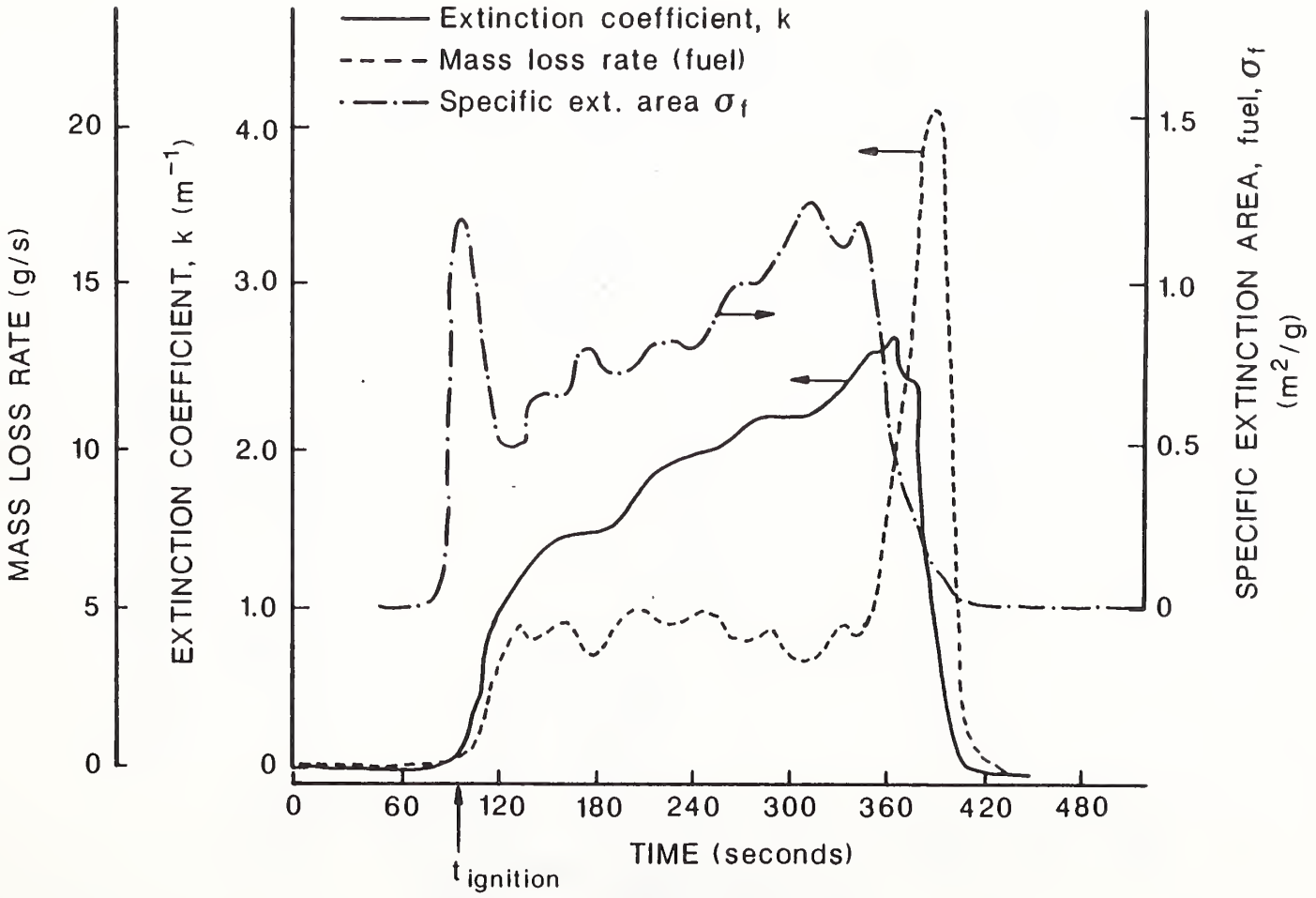

Figure 12. Mass loss rate and extinction coefficients versus time for a crude oil fire

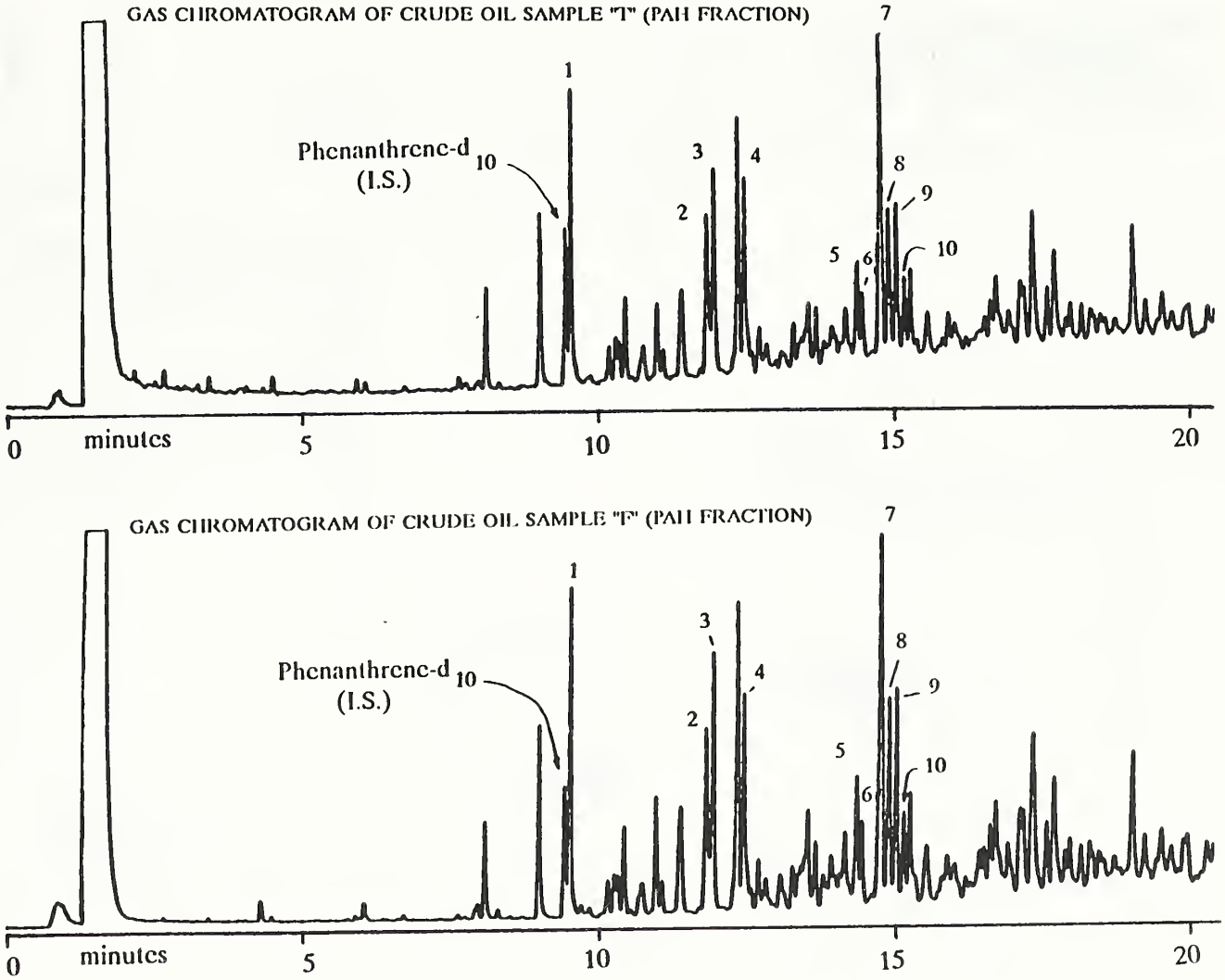

Figure 13. Comparison of gas chromatograph for Alberta Sweet crude oil and residue. Peaks: 1 Phenanthrene, 2-4 Methylphenanthrenes and 5-10 Dimethylphenanthrenes

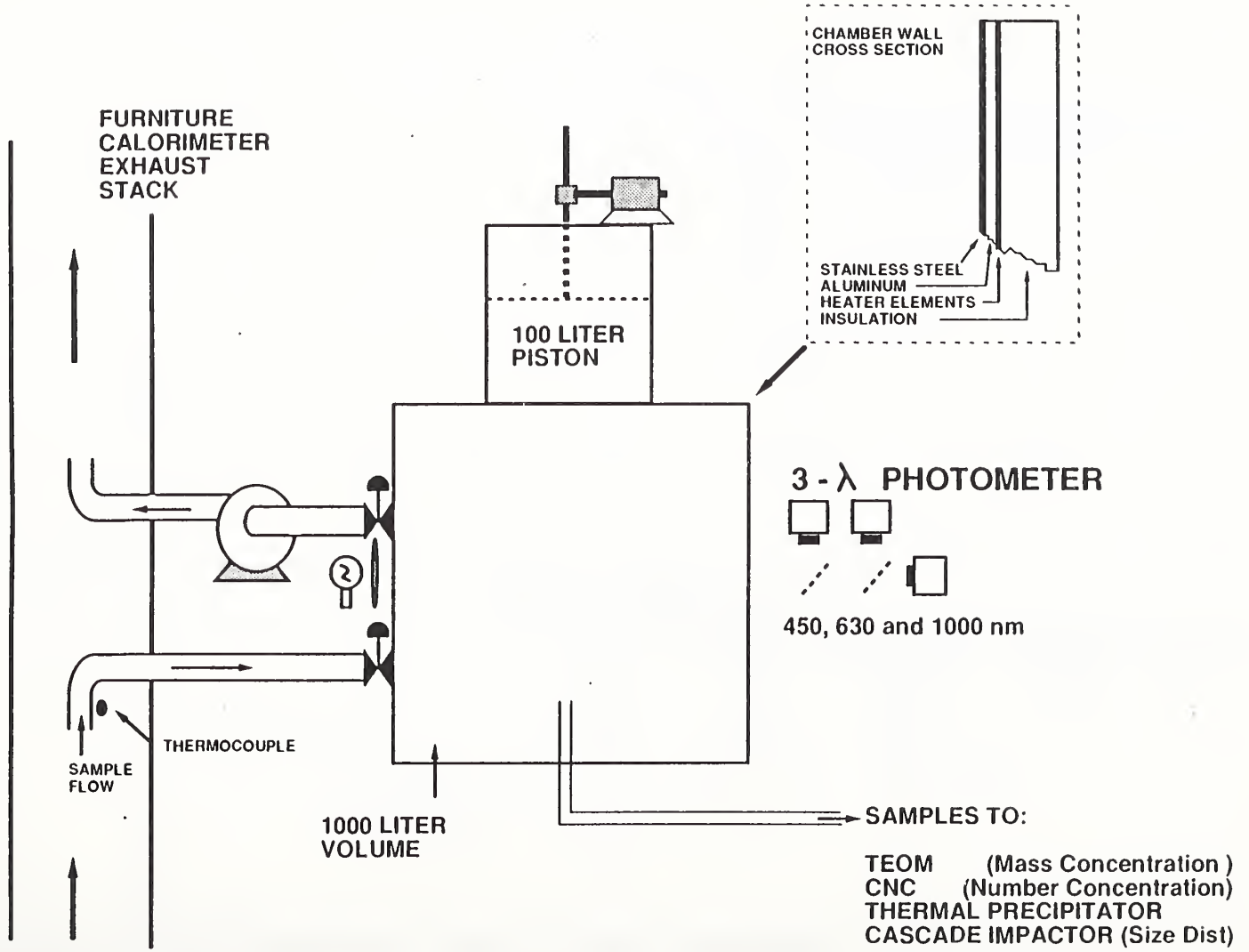

Figure 14. Smoke aging and dilution chamber (CNC - Condensation Nuclei Counter) (TEOM - Tapered Element Oscillating Microbalance)

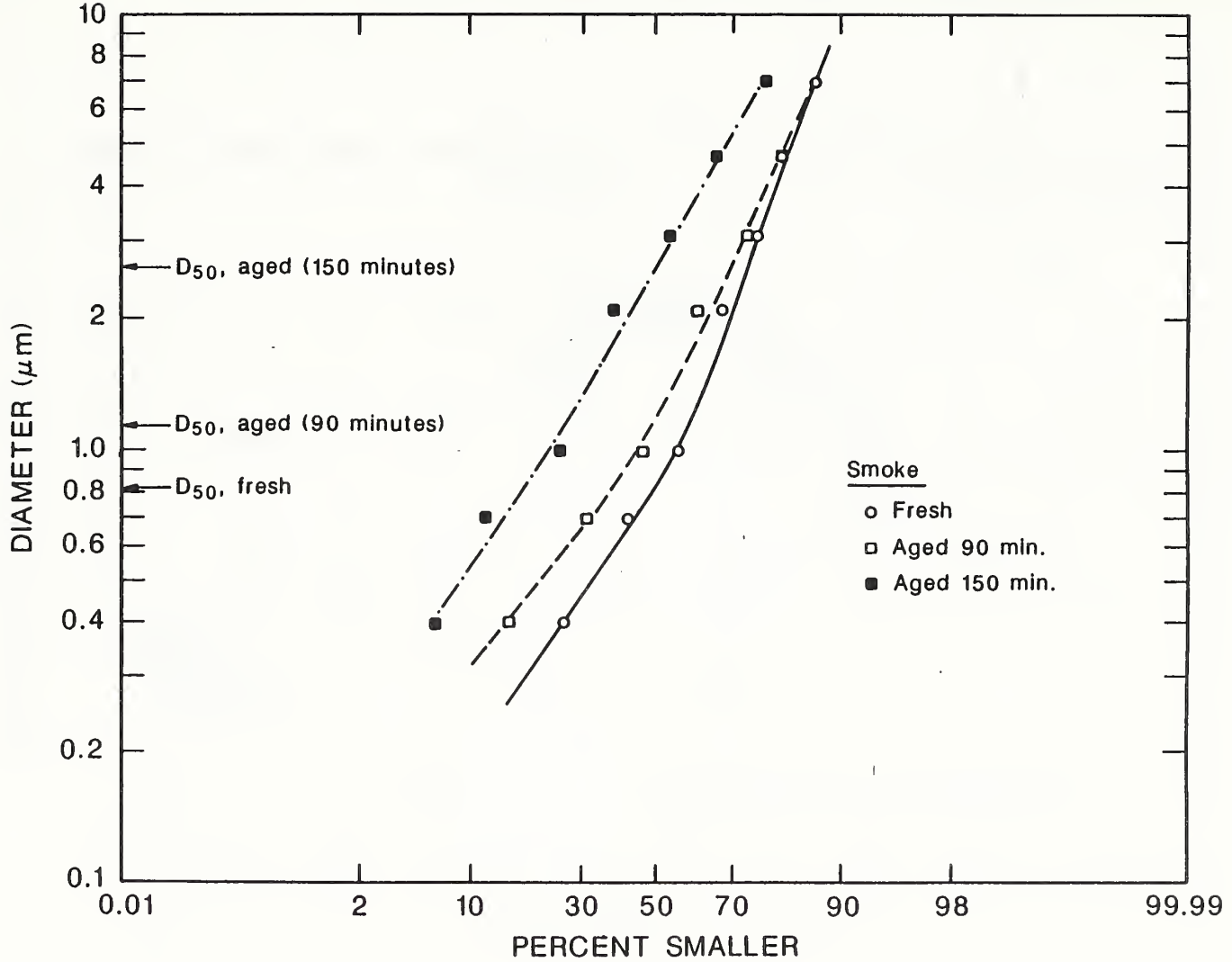

Figure 15. Effect of aging on mass distribution of crude oil smoke (log - probability plot)

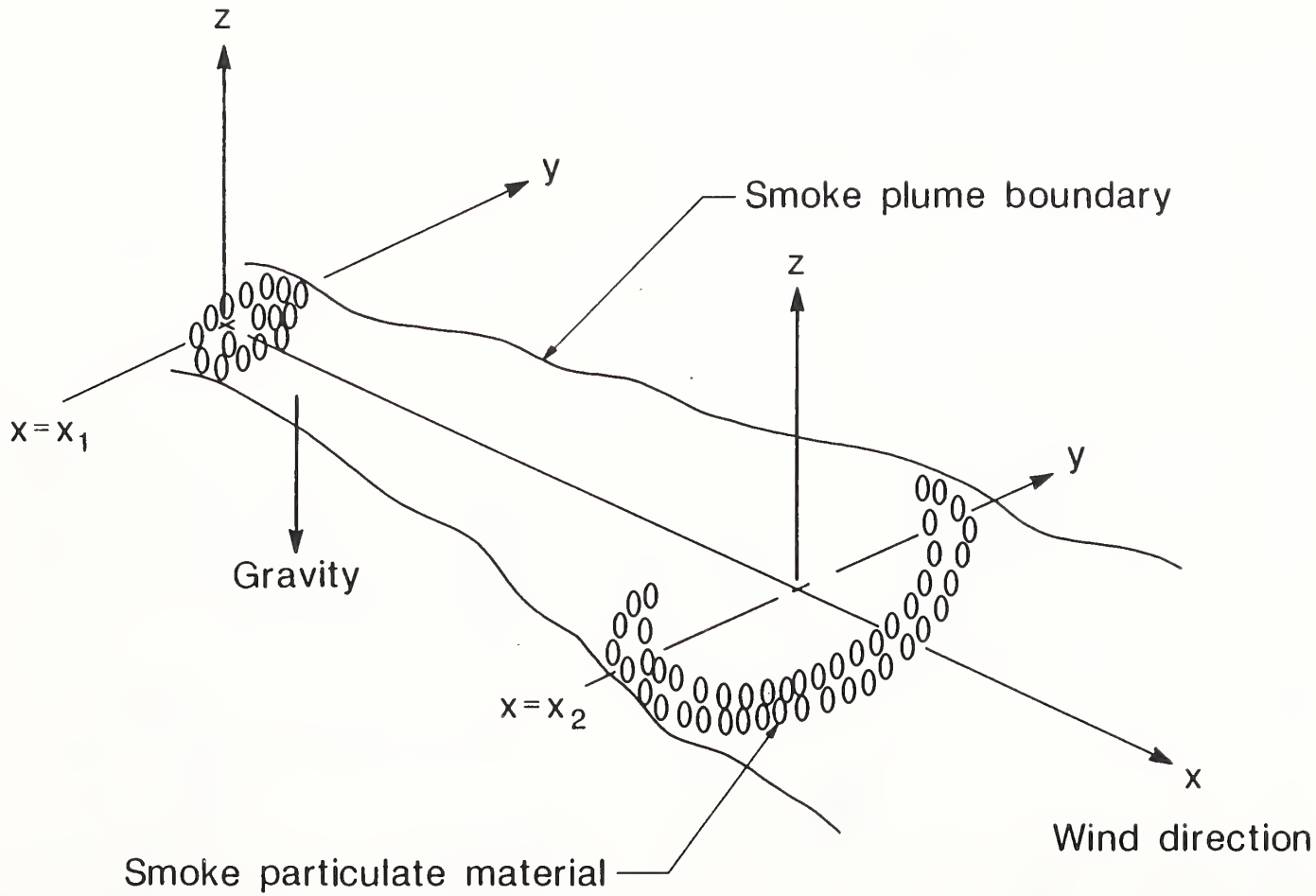

Figure 17. Schematic showing downwind evolution of smoke plume

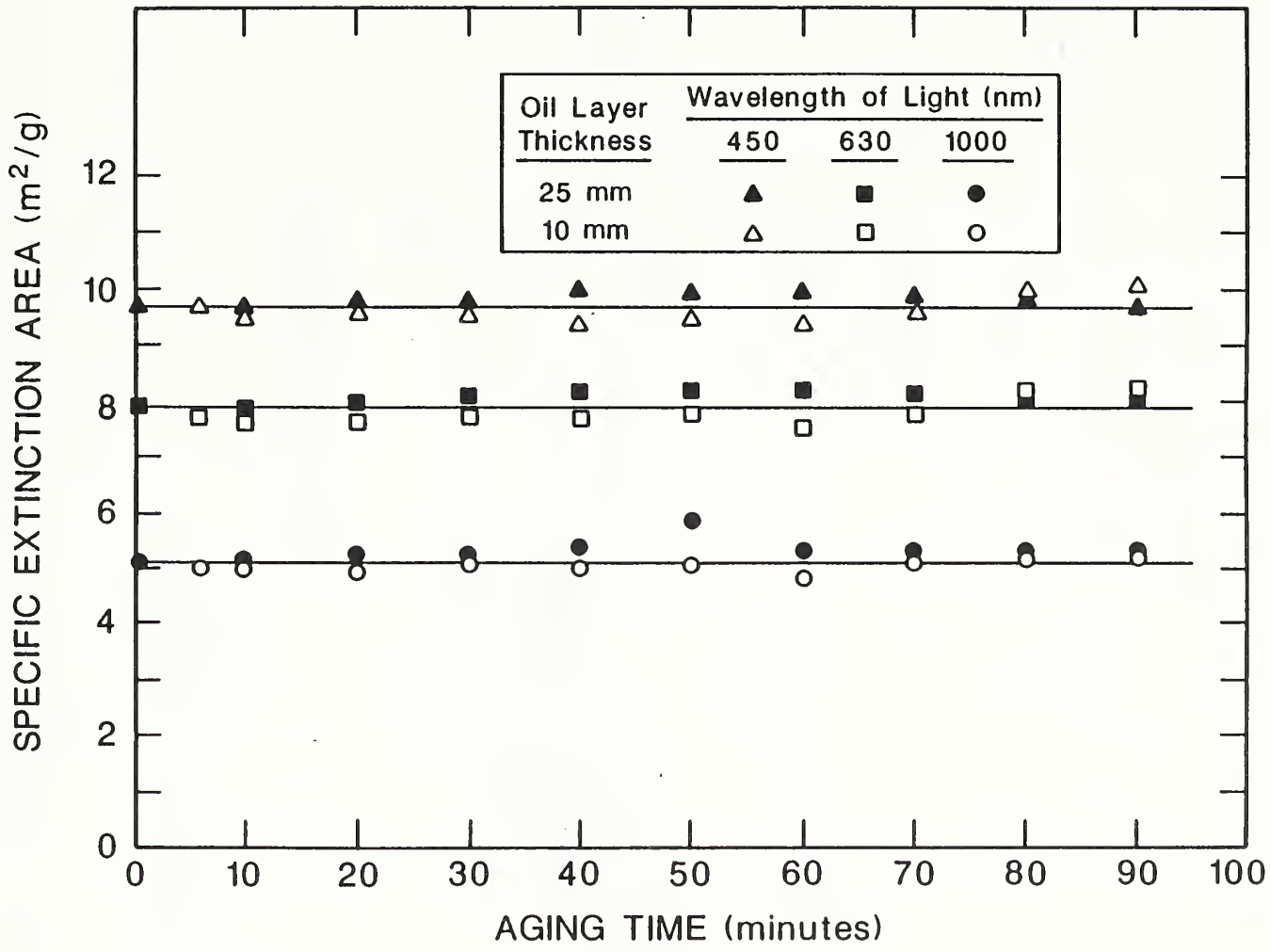

Figure 16. Effect of aging on optical properties of crude oil smoke

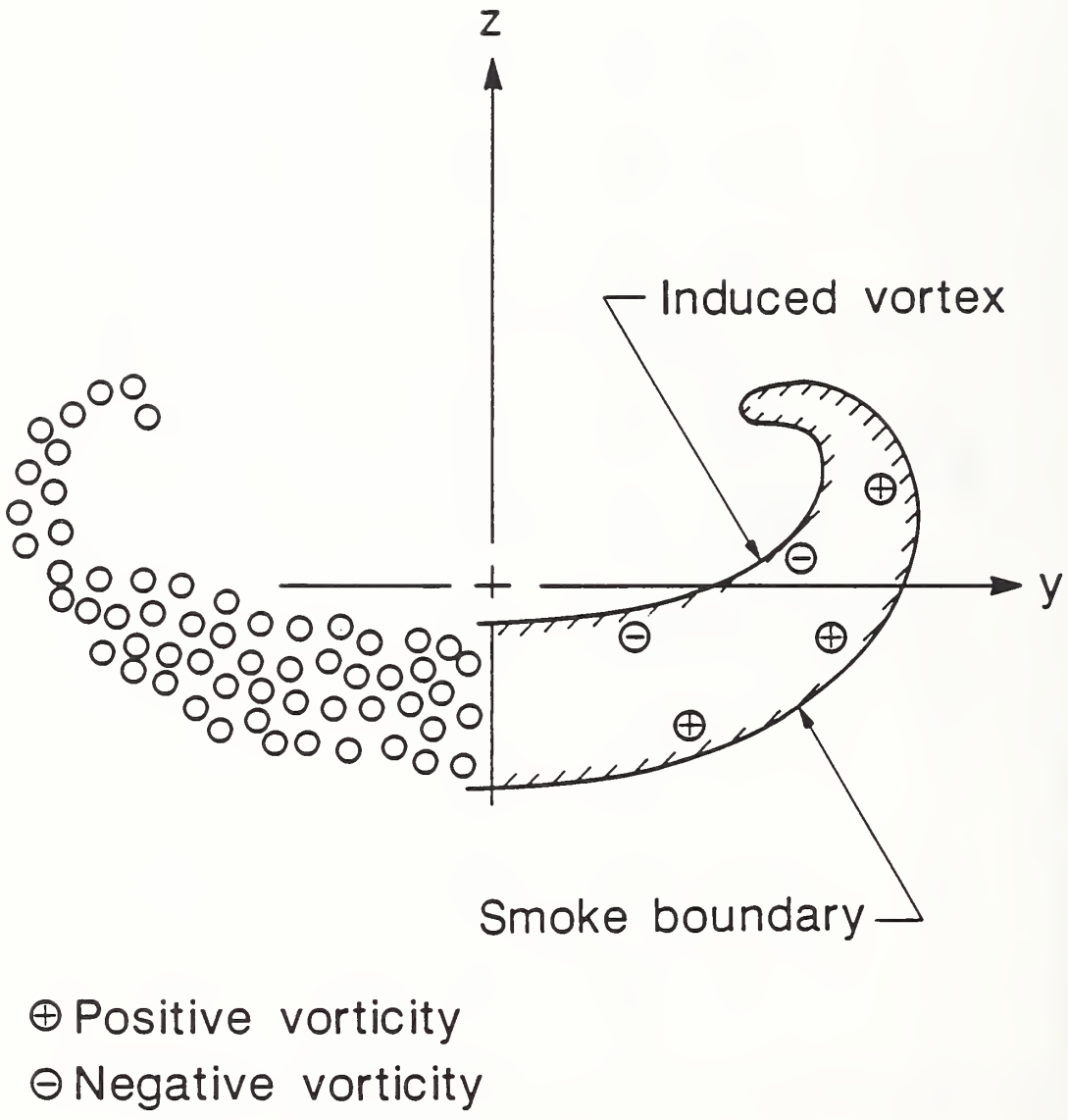

Figure 18. Discretization of smoke into vorticity containing clumps. Horizontal density gradients induced vorticity

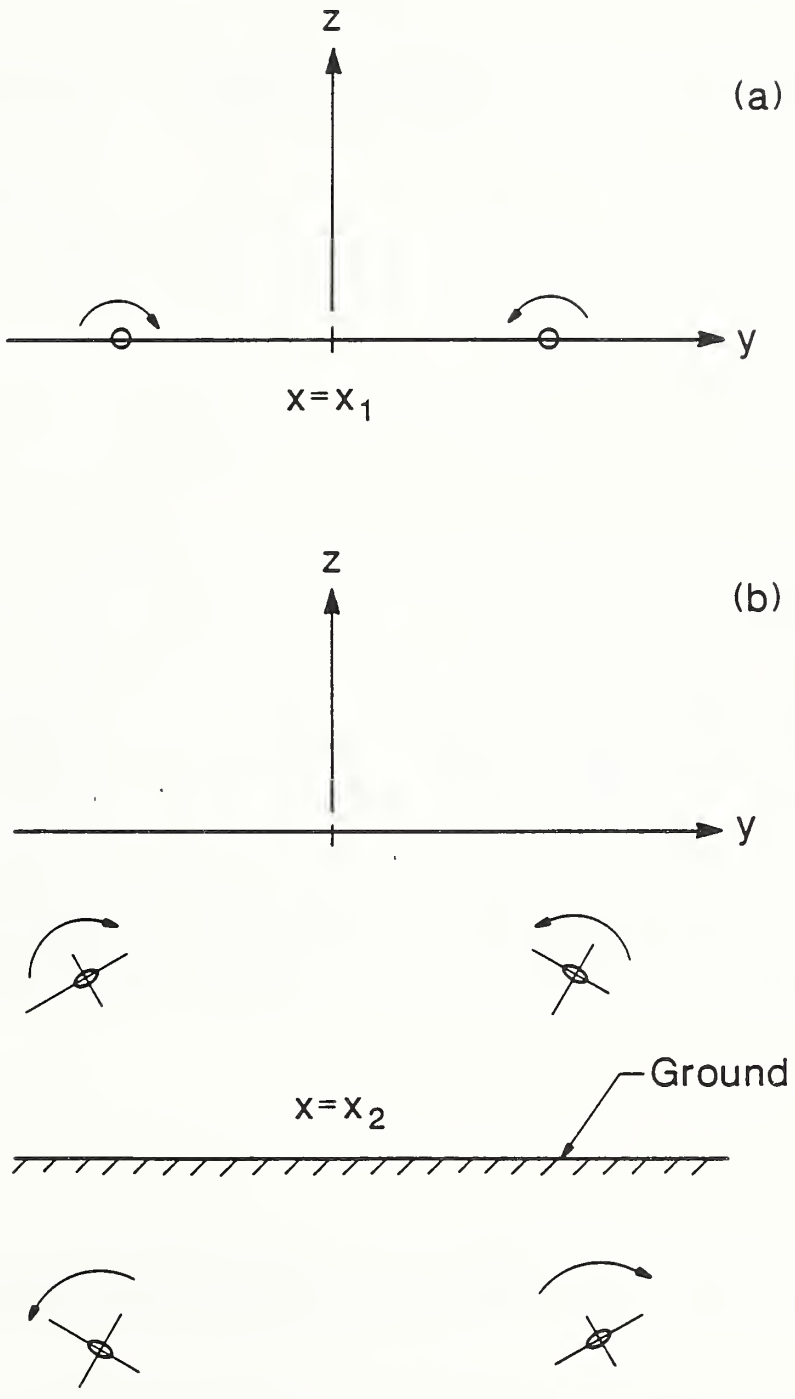

Figure 19. Fluid motion induced by vortices is indicated by direction of arrows. Ground effect is represented by image vortices

FORM NBS-114A (REV.11-84)

U.S. DEPT. OF COMM. **BIBLIOGRAPHIC DATA SHEET** *(See instructions)*	1. PUBLICATION OR REPORT NO. NISTIR-89/4091	2. Performing Organ. Report No.	3. Publication Date October 1989

4. TITLE AND SUBTITLE

Burning, Smoke Production, and Smoke Dispersion from Oil Spill Combustion

5. AUTHOR(S)

D. Evans, G. Mulholland, D. Gross, H. Baum, W. Walton

6. PERFORMING ORGANIZATION *(If joint or other than NBS, see instructions)*

National Institute of Standards
and Technology
U.S. Department of Commerce
Gaithersburg, MD 20899

7. Contract/Grant No.

8. Type of Report & Period Covered

9. SPONSORING ORGANIZATION NAME AND COMPLETE ADDRESS *(Street, City, State, ZIP)*

Minerals Management Service
U.S. Department of the Interior
Reston, VA 22091

10. SUPPLEMENTARY NOTES

☐ Document describes a computer program; SF-185, FIPS Software Summary, is attached.

11. ABSTRACT *(A 200-word or less factual summary of most significant information. If document includes a significant bibliography or literature survey, mention it here)*

The combustion of crude oil layers floated on water were studied to assess the potential of using combustion to mitigate oil spills. Burning rates for n-decane, toluene and Alberta Sweet crude oil were measured in a 1.2 m diameter pool. These were used to estimate the energy transfer rate required to vaporize the fuel as part of an energy balance at the liquid surface. Smoke emission per unit of fuel consumed was dramatically reduced in the case of burning oil layers thin enough to cause boiling in the supporting water layer. A new aging/dilution facility is described that allows for measurement of optical properties and sedimentation velocities as the smoke ages. These characteristics are important in estimating smoke properties downwind of the oil spill fire. A formulation is presented that will provide for estimates of downwind particulate deposition of the fire smoke for a steadily burning oil spill.

12. KEY WORDS *(Six to twelve entries; alphabetical order; capitalize only proper names; and separate key words by semicolons)*

crude oil; oilspills; Polycyclic Aromatic Hydrocarbons; pool fires; smoke; fire plumes

13. AVAILABILITY

☒ Unlimited

☐ For Official Distribution. Do Not Release to NTIS

☐ Order From Superintendent of Documents, U.S. Government Printing Office, Washington, DC 20402.

☒ Order From National Technical Information Service (NTIS), Springfield, VA 22161

14. NO. OF PRINTED PAGES 57

15. Price A04

USCOMM-DC 85-6006